PROPERTIES OF JOINTS IN ANVIL POINTS OIL SHALE

Submitted to:

Sandia Laboratory
Albuquerque, New Mexico 87115
Attention: Dr. Darrell Munson

Work Performed Under
Purchase Order No. 05-6021

By

Weldon W. Wilkening

TR 78-18
April, 1978

TerraTek

UNIVERSITY RESEARCH PARK · 420 WAKARA WAY · SALT LAKE CITY, UTAH 84108 · (801) 582-2220

DISCLAIMER

PROPERTIES OF JOINTS IN ANVIL POINTS OIL SHALE

Submitted to:

Sandia Laboratory
Albuquerque, New Mexico 87115
Attention: Dr. Darrell Munson

Work Performed Under
Purchase Order No. 05-6021

Submitted by:

Weldon W. Wilkening
Terra Tek, Inc.
420 Wakara Way
Salt Lake City, UT 84108

TR 78-18
April, 1978

FOREWORD

This report encompasses the work performed at Terra Tek, Inc., for Sandia Laboratories under contract number 05-6021. The principal investigator was Weldon W. Wilkening. Direct shear tests and the triaxial shear tests were completed by the principal investigator, with the assistance of Richard H. Todd. Carl E. Brechtel provided advisory assistance, especially in the early stages of the program and Cesar A. Montano provided programming assistance.

THIS PAGE

WAS INTENTIONALLY

LEFT BLANK

ABSTRACT

Properties of joints in two oil shales from Anvil Points, Colorado, containing 20 gal/ton and 40 gal/ton of kerogen, nominally, were determined by both direct shear and triaxial shear techniques. Joints tested in direct shear were oriented at 90° to the bedding plane normal and those tested in triaxial shear were oriented at 30° and 45° to the bedding plane normal. Direct shear tests were performed with constant normal stresses of 2.2, 4.4, 6.6 and 8.8 MPa, at an average shear strain rate of 5×10^{-4} sec^{-1}. Triaxial shear tests were conducted with constant normal stresses of 100 and 200 MPa, at an average shear strain rate of about 6×10^{-4} sec^{-1}.

An improved displacement transducer was developed for use in the triaxial shear tests, with which the shear and normal displacements across the joint are measured directly. Twenty gal/ton oil shale was found to be about 2 to 5 times stiffer than 40 gal/ton oil shale, in terms of both normal and shear stiffness. The 20 gal/ton shale was also found to be stronger against sliding, by a factor of about 2, and the joint properties were found to be somewhat more reproducible for the lean shale than for the rich shale.

The shear data was found to correlate well when the shear stress was normalized by the normal stress acting across the joint. The resulting shear stress/normal stress ratio vs. shear displacement plots were essentially parabolic in form, with considerable nonlinearity, even at very low shear stress levels. The lean shale slid at a constant shear stress, while the rich shale continued to "harden" during sliding.

A few direct shear tests were conducted at a strain rate two orders of magnitude higher than the rest, with no systematic variation in joint properties resulting. Also, the effect of "staging", or retesting a joint which had been previously sheared at a different normal stress level, was found to be negligible.

TABLE OF CONTENTS

THIS PAGE

WAS INTENTIONALLY

LEFT BLANK

INTRODUCTION

Direct shear and triaxial shear tests were performed on artificial joints in two grades of Anvil Points oil shale, containing (nominally) 20 and 40 gal/ton of kerogen. Normal displacements across the joint were measured during application of the normal stress, allowing determination of approximate values of the normal stiffness, K_n. Shear stress vs. shear displacement results at constant normal stress were obtained, from which approximate values for the shear stiffness, K_s, could be determined. The results of both types of measurement for both direct shear and triaxial shear tests showed that the behavior is highly nonlinear. Thus, the joint behavior cannot be adequately described by simple linear constants like K_n and K_s alone.

The direct shear apparatus used here was essentially that of Rosso[1], and Rosso, *et.al.*,[2] but with a minor modification to the normal displacement transducer configuration. The triaxial shear loading apparatus was identical to that of References 1 and 2, but the displacement transducers were totally redesigned to improve the reliability of the measurement package. The transducer configuration will be described in detail later, but it differs basically from the former[1,2] in that the normal and shear displacements across the joint are measured *directly*, rather than *indirectly* via a coordinate transformation from the radial-axial coordinate system of the cylindrical specimen. This significantly simplified the configuration, by reducing the number of individual cantilevers from eight to four, while providing complete redundancy of measurement. Whereas in the former method[1,2]

it was necessary that all eight cantilevers functioned properly in order to produce any useable data at all, only one cantilever need function in each of the two parts of the experiment (*i.e.*, normal stiffness and shear stiffness measurement) with the new transducer design. An additional benefit of the improved displacement measuring system is that extraneous motions of the specimen halves relative to one another (*e.g.*, rotation) are clearly illustrated by noting the difference between the two shear or normal displacements measured on opposite sides of the specimen. The former method[1,2] is sensitive to errors produced by such motions, but they are automatically "averaged-out" and, hence, information about them is lost. Indeed, there is no way to know whether or not rotations, etc., have occurred. With the new system, each of the displacements (normal and shear) is measured by a single cantilever on each side of the specimen. If the two shear displacements from opposite sides are vastly different, for example, severe rotation is indicated. The data can then be discarded, or averaged (if the rotation is to be ignored), or analyzed to provide insight into the shearing process, or treated in any other fashion warranted. If the two displacements are equal, or nearly equal, then it is known with certainty that the data is representative of pure sliding and the two displacements can be confidentally averaged. Some interesting observations about rotation during sliding will be discussed later.

The normal stress across the joint was held constant in each shear test, with values of 2.2, 4.4, 6.6 and 8.8 MPa for the direct shear tests, and 100 and 200 MPa for the triaxial shear tests. Normal stress in the direct shear tests was limited to that range by the strength of the ball

bearings used as a friction reducer. The average shear strain rate was $5x10^{-4}$ sec^{-1} for direct shear and about $6x10^{-4}$ sec^{-1} for triaxial shear tests, although a few direct shear tests were performed at an average shear strain rate two orders of magnitude higher, to assess the effect of strain rate on the joint shear properties.

All of the triaxial shear specimens which survived the first shearing process were subjected to "staging" — they were retested at the other value of normal stress, to assess the influence of prior sliding upon the shear properties.

Direct shear tests were performed on cores whose axes were oriented parallel to the bedding plane normal, while triaxial shear tests were performed on cores with their axes at 45° or 60° to the bedding plane normal. In accordance with the orientation nomenclature of the contract sponsor, the specimens were referred to by the complement of the angle between the joint plane normal and the bedding plane normal. Hence, direct shear specimens contained 90° joints, and triaxial shear specimens contained 45° or 30° joints.

EXPERIMENTAL PROCEDURE

Specimen Preparation

Rectangular prismatic pieces of oil shale, approximately 50 mm by 200 mm by 75 mm were scored on all four sides in the plane of the planned joint. Scoring was performed with a 1.5 mm thick diamond blade; depth was about 10 mm for the scores perpendicular to the front and back faces and about 15 to 20 mm for the scores entering the side faces at an angle. This was necessary to improve the probability of extending the joint along the correct plane, rather than curving into the bedding planes, at the edge of the specimen. The scored blocks were then split with a pair of 60° wedges. Approximately two thirds of the splits were successful — many failed because of excessive bedding plane splitting. Pieces which broke off from the joint surface due to bedding plane splitting were reattached with Devco 5-Minute Epoxy, if no small fragments were missing. The joints were then glued back together with Duco cement and held in a clamping jig for 1 to 2 days while the cement dried.

Cores were then cut from the cured, pre-split blocks, using water as coolant. All cores were cut with their axes parallel to the bedding plane normal — 51 mm (2 inch) cores were used for direct shear and 37 mm (1-1/2 inch) cores were used for triaxial shear. After coring, the specimens were cut to length and the ends were surface ground flat and parallel. The Duco cement was completely removed from the joints with acetone. Some of the specimens separated during coring; they were cleaned and held back together temporarily with tape while the ends were ground. No significant difference was noted in the precision resulting from the two techniques.

Direct Shear Testing

Figure 1(a) is a schematic diagram of the direct shear apparatus, as used by Rosso[1] and by Rosso, *et.al.*[2] Figure 1(b) is a photograph of a sheared specimen, mounted in the shear boxes. To obtain accurate alignment of the two specimen halves in their separate shear boxes, one half was first mounted in its box with grout and the grout allowed to harden. Then the other half was mounted in its box and the first shear box was quickly mounted in place on top and clamped into correct alignment while the grout in the second box hardened.

Figure 1 shows that two shear cantilevers are attached to the bottom shear box — the short transducer measures the displacement of the bottom half of the specimen relative to the bottom shear box and the long transducer measures the displacement of the top half of the specimen relative to the bottom shear box. The two signals are recorded separately and the relative shear displacement of the two specimen halves is computed by taking the difference in the transducer outputs after the experiment. In the experiments reported here, the short shear displacement was typically less than 10 percent of the long shear displacement, because the shear box was considerably stiffer than the joint being tested. The two shear cantilevers are visible in the photograph of Figure 1(b). Figure 1(b) also shows clearly the rings which are attached to the specimen with four set screws. The rings support the normal displacement transducers and the transfer rods which contact the shear displacement cantilevers. In Figure 1(a), the side view of the normal displacement transducer shows that two cantilevers were employed on each side of the specimen.[1,2] In

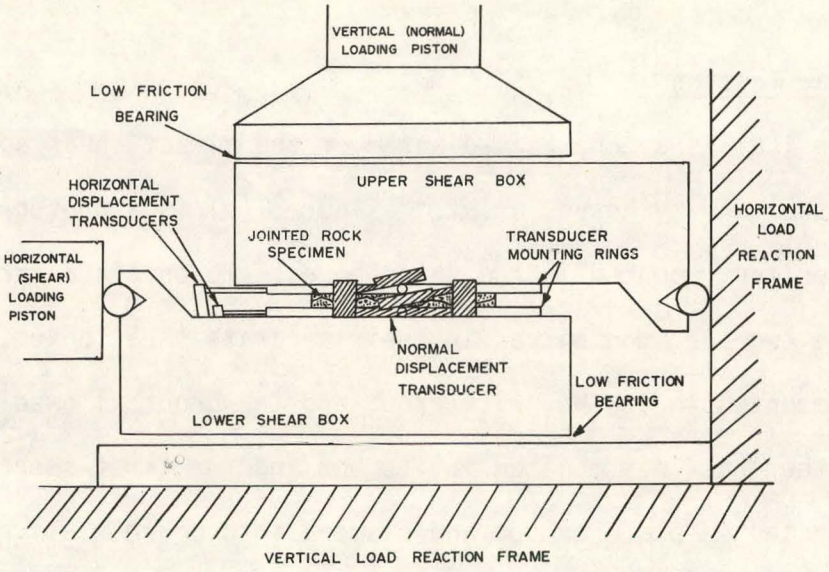

1A

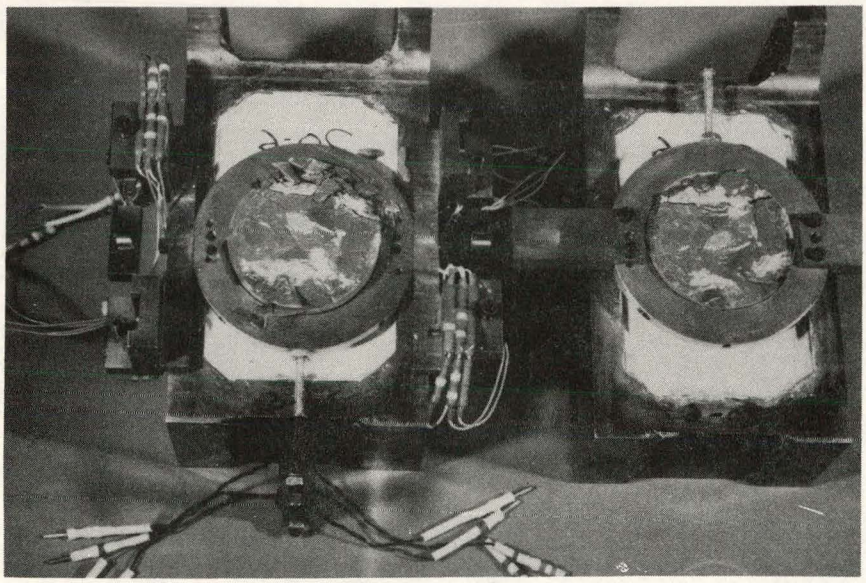

1B

Figure 1. Direct shear apparatus. a) Schematic of direct shear testing apparatus, as used by Rosso[1]. b) Direct shear specimen after testing, showing modified method of measuring normal displacement with a single cantilever on each side of the specimen.

the experiments reported here, however, only one cantilever was used on each side to eliminate problems associated with pre-loading the cantilevers.

Specifically, with two operative cantilevers, only half the linear range of deflection of either of the two nominally identical cantilevers is available for use, since one must relax while the other deflects further. Should the former approach its relaxed position, the output of the pair will become bilinear, reaching half its original sensitivity as one cantilever relaxes totally. Excessive pre-loading eliminates the problem, but raises the possibility that the other cantilever will be driven past its linear range during testing. In either case, one cannot be sure what is happening, since the two signals are, again, automatically averaged by virtue of having the two cantilevers wired into the same Wheatstone bridge circuit. The justification for such a design came, in the first place, from recognition of the fact that the effective length of either cantilever will change as sliding occurs, resulting in a nonlinear transducer. The back-to-back cantilever configuration neatly overcomes the potential problem, however, since the output of the pair (if properly pre-loaded) is independent of the position of the pin against which the cantilevers rest (*i.e.*, independent of the sliding displacement). Unfortunately, this advantage was not previously recognized, but rather it was assumed that the sensitivity was still a function of the relative shear displacement. Consequently, a computer program was written to continuously calculate the sensitivity during sliding.[2] It now appears that the observed nonlinear behavior of the original transducer was very probably the result of the pre-loading problem discussed above.

For the present work, only one cantilever was used on each side, to double the deflection range available. Also, since the normal displacement was not to be measured during sliding anyway, the importance of the dependence of effective cantilever length upon sliding displacement is a moot point.

The normal and shear loads were measured with hollow cylindrical load cells, each instrumented with four strain gages, so each load cell was a complete Wheatstone bridge circuit, as were the two shear cantilevers (each cantilever was instrumented with a pair of strain gages on each side of the reduced section). Each of the normal displacement transducers was also a full bridge circuit, although in the configuration employed here, only two gages were active. All strain gages were 350Ω, and all bridge circuits were excited with 5V. Both load signals were amplified with a gain of 1000, and all centilever signals were amplified with a gain of 2000. Calibration of all cantilevers was accomplished by measuring the voltage output from the amplifier as a function of displacement over the entire linear range of the transducer, the displacements being measured with a dial gage. The voltages produced by several shunt resistors internal to each of the amplifiers were then measured also and the value of displacement corresponding to each shunt resistor value was then computed from the least squares fit to the voltage vs. displacement data. The average values from three separate calibrations runs were used, each with coefficient of determination of at least 0.999. The load cells were calibrated in an analogous fashion, but the loads were measured with a U.S. Bureau of Standards traceable 50,000-pound Morehouse Ring Dynamometer.

The loading apparatus, shown schematically in Figure 1(a), consisted of a small servo-hydraulic load frame, with a 100,000-pound actuator, and a separate horizontal load frame with a 20,000-pound actuator. The large vertical actuator was operated in load control, while the smaller horizontal actuator was operated in displacement control. The normal load was increased, with no shear load, to the value required for the direct shear test. During this loading the normal displacements were monitored, to determine the normal stiffness of the joint. Then, with the normal stress held constant, the shear ram was ramped toward the reaction frame, to produce the required shear displacement. Both loads and the two shear displacements were monitored during this part of the test. Data was recorded automatically with a PDP-11/34 real-time data acquisition system, with data being taken at specified intervals in the normal load signal for the first (normal stiffness) part of the test and at specified intervals in the shear load signal for the shear portion of the test. After sliding commenced, and the shear load reached an essentially constant value, the data acquisition program called for data at specified intervals of time.

In order to monitor the progress of the test, the two loads and the large shear displacement were also recorded on an X-Y-Y' recorder. After the experiment, a reduction program was run on the data to compute stresses from the measured loads and to compute the relative shear displacement and the average normal displacement. Unfortunately, it was discovered that the data acquisition program, which was that used in References 1 and 2, contained an error which resulted in deletion of the data from channel 4 (the short shear displacement) and the shifting of the data from channels 5 and 6

(the normal displacements) to columns 4 and 5, respectively. Some of the direct shear tests were repeated after the correction to the data acquisition program had been made and no significant difference was noted between the data from the repeated tests and the correctly reprocessed data from the original direct shear tests.*

Triaxial Shear Testing

Triaxial shear tests were conducted in a 4 Kb vessel, mounted on the upper platen of a test frame equipped with a 130,000-pound actuator. The 37 mm (1.5 inch) diameter specimen, containing an artificial joint at either 30° or 45° orientation, was pressurized and then sheared by ramping the vertical actuator downward. As shown in Reference 1, the stresses acting on the joint surface are given by the following expressions:

$$\sigma_n = p + (\sigma_1 - p) \sin^2 \alpha \qquad \text{(Normal stress)}$$

$$\tau = (\sigma_1 - p) \sin \alpha \cos \alpha \qquad \text{(Shear stress)}$$

where α is the complement of the angle between the specimen axis and the joint plane normal, p is the confining pressure and σ_1 is the total axial stress. The stresses are written in terms of pressure, p, and differential axial stress, $(\sigma_1 - p)$, since those are the quantities measured directly by the pressure transducer and axial load cell, respectively.

Now, to keep σ_n constant during the test, while increasing τ, it is necessary to decrease p in proportion to the increase in $(\sigma_1 - p)$, as seen from the following:

$$\frac{d\sigma_n}{dt} = \frac{dp}{dt} + \frac{d(\sigma_1 - p)}{dt} \sin^2 \alpha = 0$$

therefore, $dp/dt = - \sin^2 \alpha \, [d(\sigma_1 - p)/dt]$ must be satisfied, or

$$\frac{dp}{d(\sigma_1 - p)} = \frac{dp/dt}{d(\sigma_1 - p)/dt} = - \sin^2 \alpha$$

For $\alpha = 45°$, $\sin^2 \alpha = 1/2$, and for $\alpha = 30°$, $\sin^2 \alpha = 1/4$. In these experiments, the axial load increased monotonically due to the motion of the vertical actuator, which was ramped downward under displacement control. The differential axial load and the pressure were plotted on an X-Y recorder, pressure being controlled by operating the pressure intensifier ram in displacement control. The setpoint on the pressure servo controller was manually turned down to make the pressure-axial load relationship follow the path of constant σ_n. The pressure was generally maintained to within about 10 percent of the proper value, except for some of the unloading-reloading cycles to be described later, for which 20 to 25 percent deviations occurred at the point of load direction reversal.

Figure 2(a) shows the displacement transducers developed for this testing program. The normal and shear cantilevers were bolted together to form a single unit, one for each side of the specimen. The four leads from each cantilever were connected to an IC socket, which served as a receptacle for the transducer pair. Each cantilever was 25 mm in length (1 inch), exclusive of the 12.5 mm (0.5 inch) square block which served as a mounting block for the pair. Half the length of each cantilever was reduced in thickness and

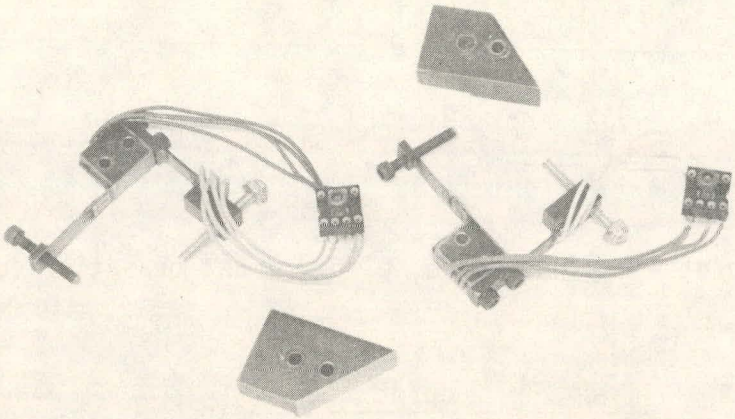

2A

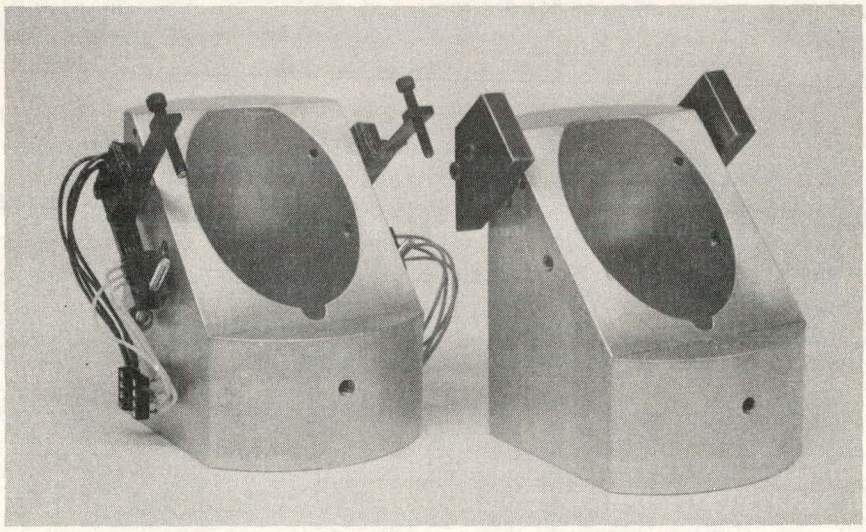

2B

Figure 2. Triaxial shear displacement transducer system. a) Normal and shear cantilever units and associated reference blocks. Each cantilever is a full Wheatstone bridge circuit, with two strain gages on either side of the reduced section. b) Cantilever units mounted on rings. The reference blocks are mounted on one ring and the cantilever units are mounted on the other. One pair of rings was made for each joint angle. (The 45° rings are shown).

contained a pair of 350Ω strain gages on each of its faces, thereby making each cantilever a complete bridge circuit, with four active gages. The reduced section of the normal displacement cantilevers was 0.9 mm (0.035 inch) thick and that of the shear displacement cantilevers was 0.4 mm (0.016 inch) thick. Those dimensions resulted in linear displacement ranges of 0.6 mm (0.025 inch) and 2.5 mm (0.100 inch), respectively. A small adjusting screw at each cantilever end allowed pre-loading the cantilevers prior to testing. Figure 2(b) shows the two transducers mounted on the aluminum support rings — cantilevers on one ring and fixed reference blocks on the other. The figure shows that the shear displacement cantilevers were mounted such that the reference blocks moved *away from* the cantilevers during sliding, to protect the transducers, should excessive sliding occur. The normal displacement cantilevers were operated in the opposite mode during the hydrostatic loading portion of the test. The screw holes visible on the support rings in Figure 2(b) are for mounting the support rings on the specimen. A short (∿3 mm) rod was inserted in each of the four holes on each ring and sealed against the side of the specimen with silicon rubber. An Allen head set screw, with a 1 mm diameter hole drilled down its axis, was screwed into the hole and tightened against the rod to hold the ring firmly onto the specimen. When the specimen contracted radially during pressurization, causing the set screw to loosen, the confining pressure, acting on the exposed end of the short rod, provided the force holding the rings to the specimen.

Figure 3 shows the several steps involved in preparing the jointed specimens for triaxial shear testing. Figure 3(a) shows the specimen, with end caps attached, and coated with an inner jacket of bookbinding wax. The

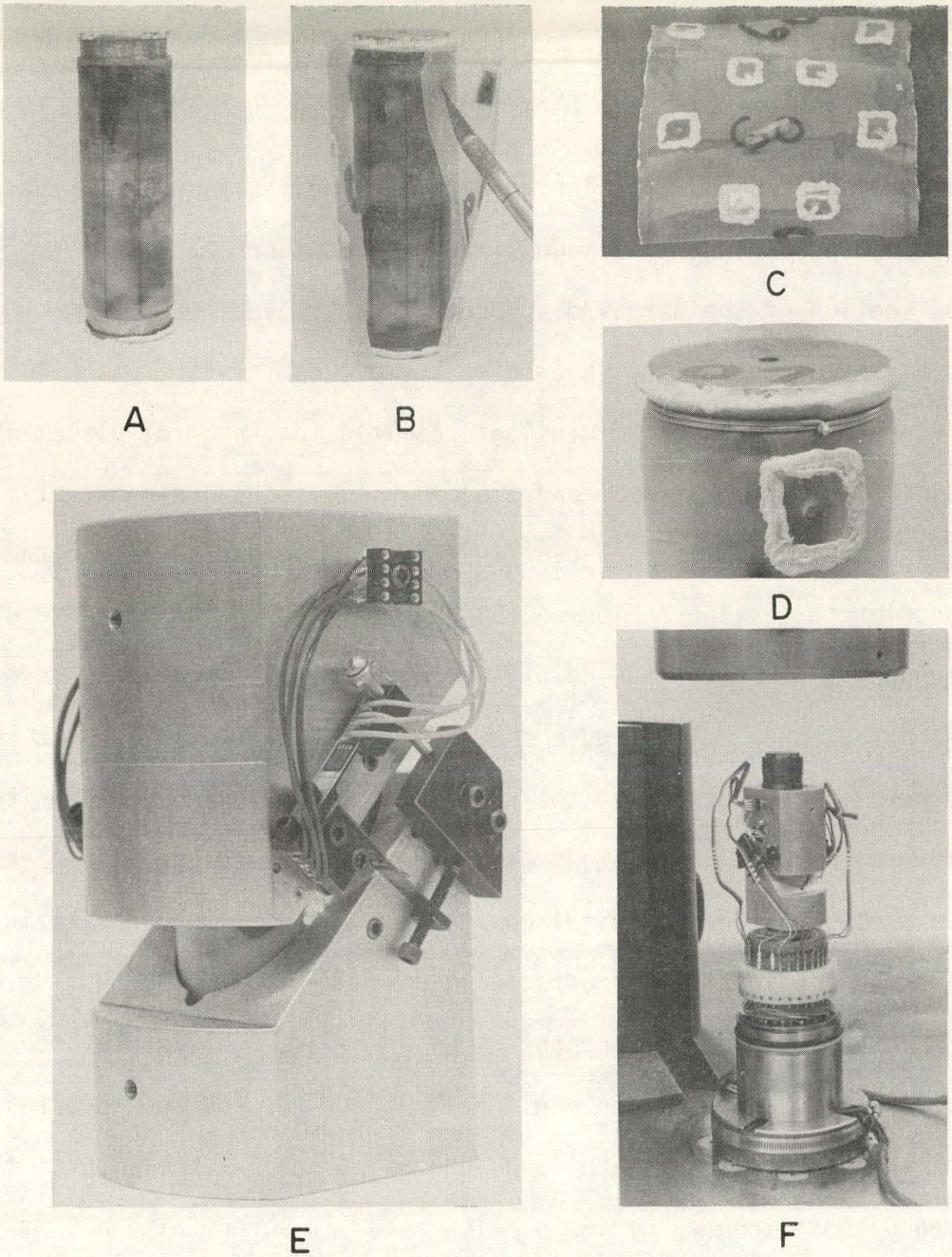

Figure 3. Sequence of preparation of triaxial shear specimens. a) Specimen coated with bookbinding wax, with steel endcaps epoxied in place. b) Cutaway view of outer double polyurethane jacket. c) Outer jacket, illustrating placement of stainless steel shim pads which distribute the load from the set screws which hold the transducer rings in place. d) Close-up of the jacketed specimen, showing how the edges of the shim pads are sealed with a bead of room-temperature-vulcanizing silicon rubber and illustrating the method of sealing the jacket to the steel endcaps with stainless steel lockwire. e) Completed specimen with transducer rings attached. The plug at the top provides electrical connection to the strain gages on the cantilevers. f) Specimen mounted on base plug, ready to be raised into the pressure vessel for testing. The cantilever leads are connected to high-pressure cone feed-throughs near the bottom of the base plug. The axial load cell is beneath the specimen. Note the low-friction bearing atop the specimen.

wax was found to be ideal for the purpose, because it was easy to apply, it sealed very well, was pliable enough under pressure to maintain its sealing capacity even after sliding, and it had just the right stiffness to complement the hydraulic-pin method of attaching the rings to the specimen. Figure 3(b) shows a cut-away view of the outer jacket, comprised of two layers of polyurethane sheet. Figure 3(c) shows the outer jacket, removed from the specimen and spread out to illustrate the placement of 10 mm square pads of 0.1 mm thick stainless steel shim stock under the hydraulic pins, to distribute the high loads at the pins over a larger area. Figure 3(d) is a close-up of the jacketed specimen end, showing the method of sealing the polyurethane outer jacket to the end caps with stainless steel lockwire and again showing one of the load-distributing pads. The completed specimen, with rings and displacement transducers mounted ready for testing, is shown in Figure 3(e), and the specimen is shown mounted on the base plug of the pressure vessel, ready for insertion, in Figure 3(f). The cylinder on top of the specimen in Figure 3(f) is the friction reducer, which consists of two mirror-polished metal surfaces, lubricated with a grease made from MoS_2 powder in vacuum grease.

The four displacement transducers were calibrated in a manner analogous to that employed for the direct shear displacement transducers. The pressure transducer, a 350Ω manganin coil, was wired into a Wheatstone bridge circuit and calibrated in a similar manner, with the pressure being measured with a 60,000 psi Heise gauge. The axial load cell, which was mounted directly under the specimen, was instrumented with eight 350Ω strain gages, forming a full 700Ω Wheatstone bridge circuit. It was calibrated just as

the load cells for the direct shear tests, using the same 50,000-pound Morehouse Ring Dynamometer. The load cell signal was amplified by a gain of 200, as were the shear displacement signals. The pressure signal was amplified by a gain of 1000 and the normal displacement signals by a gain of 500. All calibration data, as well as test data, was taken with the PDP-11/34 real-time data acquisition system, just as in the direct shear testing program. The corrected "timed data acquisition" program was used for all but the first half-dozen triaxial shear tests, with data being taken at specified intervals in the pressure signal for the normal stiffness experiment, and at specified intervals in the axial load signal for the shear stiffness experiment. Again, as sliding commenced, data was taken at specified intervals of time.

RESULTS AND DISCUSSION

Direct Shear

The results of normal stiffness measurements made on the direct shear specimens, prior to shearing, are illustrated in Figure 4. At the low normal stress level involved, the normal stress vs. normal displacement relationship is seen to be quite linear, especially for the 20 gal/ton oil shale. The normal stiffness, K_n, is about 50 MPa/mm for the lean shale, and about 10 MPa/mm for the 40 gal/ton shale. There is, however, evidence of increasing normal stiffness with increasing stress in the 40 gal/ton oil shale. It is also noteworthy that the scatter is considerably greater in the richer shale. This trend will be seen to persist throughout all the data acquired in this program.

Figures 5 and 6 illustrate the shear stress vs. shear displacement results for 20 gal/ton and 40 gal/ton oil shale direct shear tests, respectively. In these figures, the shear stress has been normalized by the normal stress, which results in collapsing all the curves into a single band, for each material. There is still considerable scatter, but the underlying trend is clear. Because of the scatter and the pronounced non-linearity in the curves, it is difficult to define a single linear-elastic parameter, such as shear stiffness, K_s. If the curves were to be analyzed separately (as presented in Figures C-1 through C-5, Appendix C) it would be noted that even more (apparent) scatter exists — curves even cross each other, for example. But it is reasonable that the shear stress should scale with the applied normal stress (indeed, it is common to rate joints in terms of the "coefficient of friction" at sliding, which is nothing but the stress

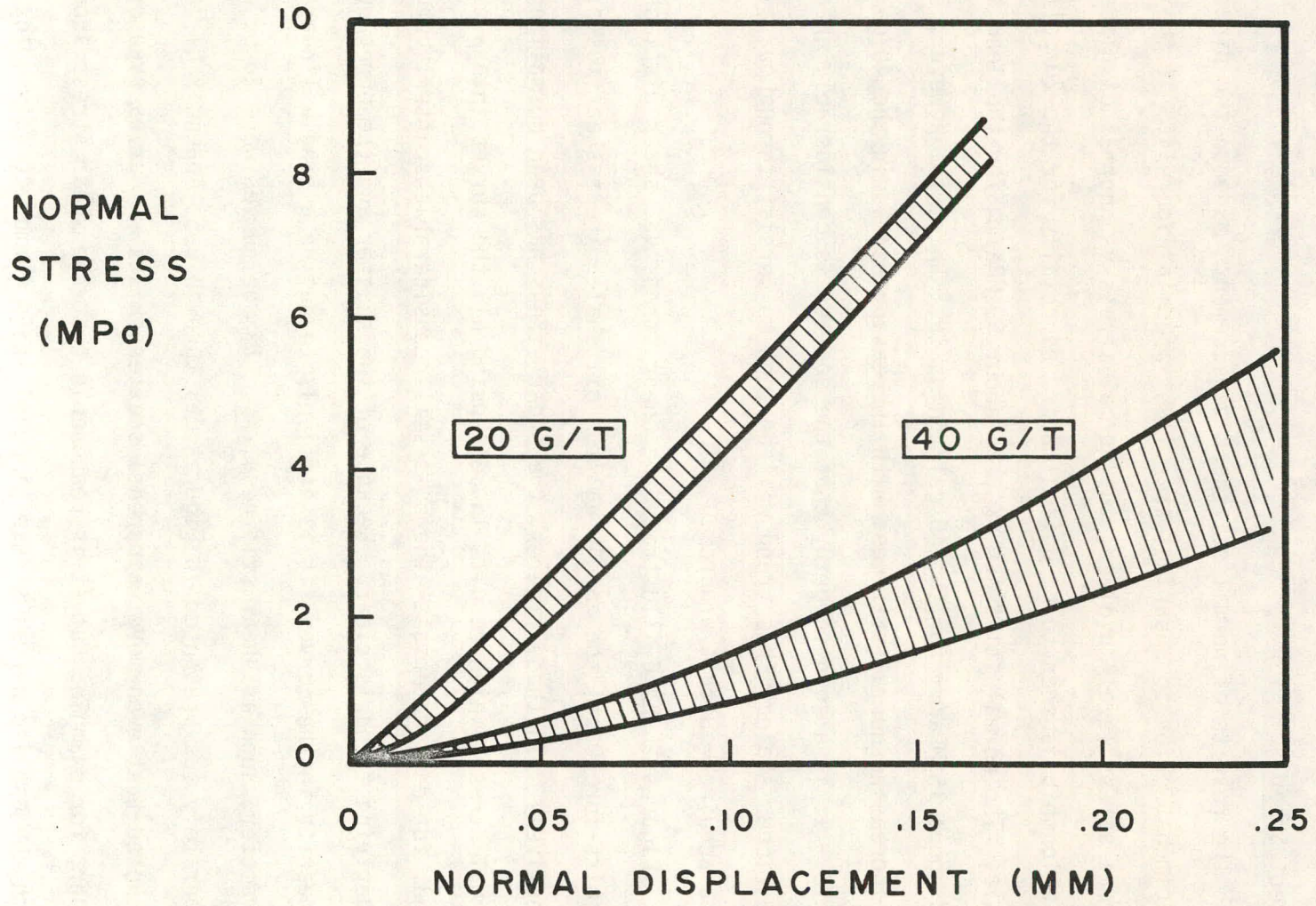

Figure 4. Normal stiffness results for direct shear specimens.

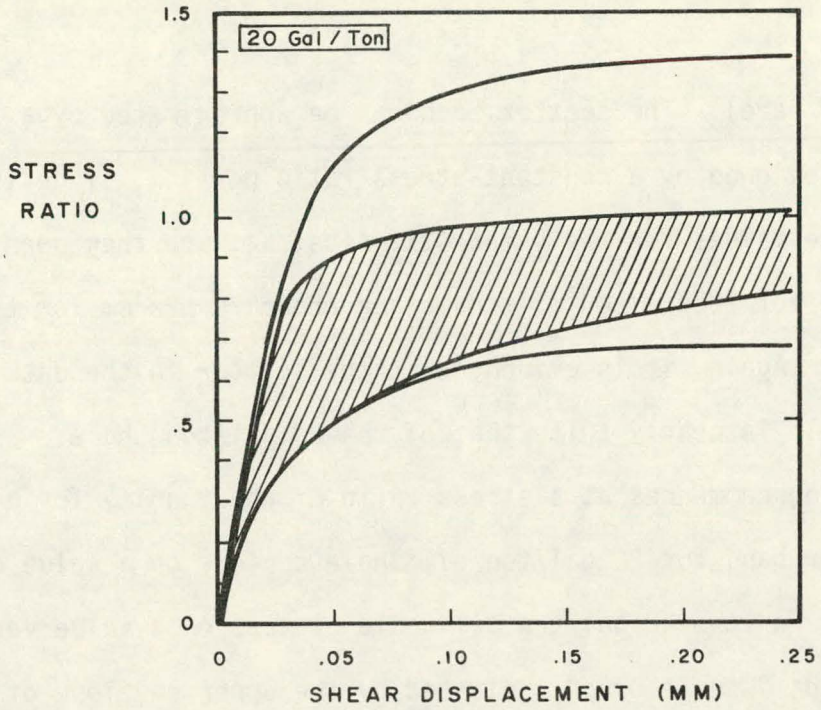

Figure 5. Direct shear results for 20 gal/ton oil shale. Stress ratio is the ratio of shear stress to normal stress. The shaded band is the envelope of all "slow" tests, while the solid curves are results of "fast" tests.

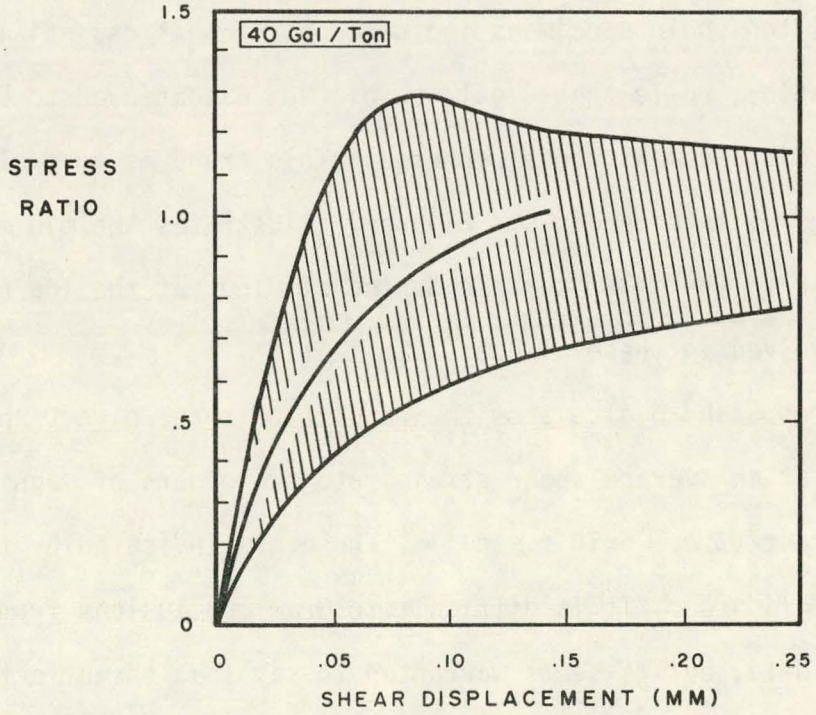

Figure 6. Direct shear results for 40 gal/ton oil shale. Stress ratio is the ratio of shear stress to normal stress. The shaded band is the envelope of all "slow" tests, while the solid curve is the result of the "fast" test.

ratio used here). The scatter band can be approximated by a linear elastic portion, followed by a constant-stress ratio portion, if desired. The approximate values for the shear stiffness, K_S, are then seen to be about 125 MPa/mm for 20 gal/ton oil shale and about 70 MPa/mm for the 40 gal/ton oil shale. Again, it is evident that the scatter in the data for the richer shale is nearly twice that of the 20 gal/ton shale.

Sliding commences at a stress ratio of about unity for both shales — the scatter band for 20 gal/ton oil shale centers on a value of about 0.8, while that for the 40 gal/ton oil shale centers on a value very near 1.0. The apparent "stress drop" indicated by the upper envelope of the richer shale's scatter band was indicated in only a single test — most of the curves for both materials were smooth and parabolic in form. What the scatter bands in Figures 5 and 6 do not illustrate well is the fact that the 20 gal/ton shale specimens indicated sliding at essentially constant stress (ratio), while the 40 gal/ton oil shale continued to "harden" over the shear displacement range recorded. This trend is more clearly shown in the figures in Appendix C. Figure 7 illustrates the minimal amount of damage done to the joint surface during sliding, at the low normal stress levels involved in these direct shear tests.

Figures 5 and 6 also show the results of three direct shear tests performed at an average shear strain rate two orders of magnitude higher than the rest (*i.e.*, 5×10^{-2} sec^{-1}). These are indicated by the solid lines in the two figures. It is difficult to draw conclusions from such a limited amount of data, but it seems warranted to say that the effect of strain rate is negligible. The two "fast" shear results for 20 gal/ton shale fall outside

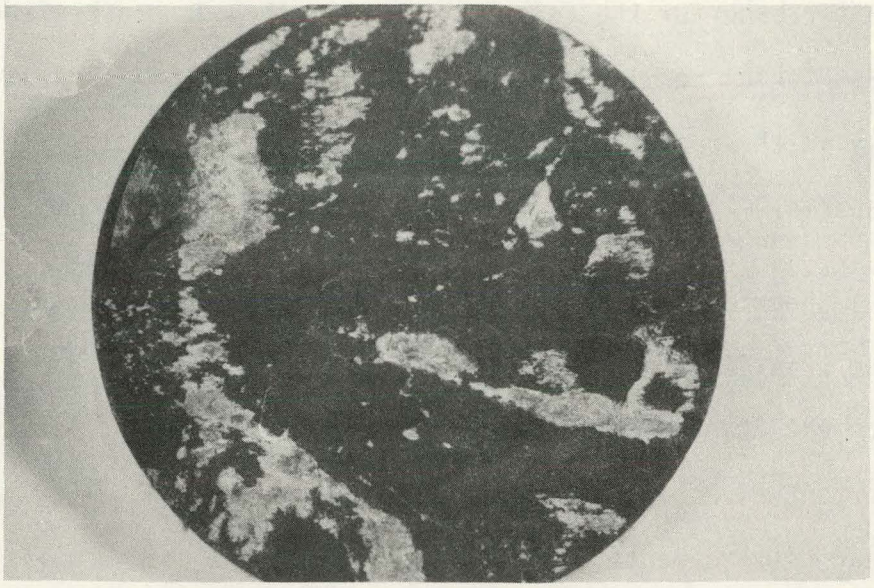

7A

7B

Figure 7. Representative joint surfaces after direct shear testing. a) 20 gal/ton. b) 40 gal/ton. Note that at the low normal stresses involved in direct shear testing, only minimal surface asperity crushing occurs.

the scatter band for the "slow" tests, but they do bracket the same band. The "fast" shear result for the single test on 40 gal/ton oil shale falls directly in the center of the scatter band from the "slow" tests on the same material.

Triaxial Shear

The triaxial shear tests were conducted with the use of the improved displacement transducer described in the Introduction. As mentioned there, an important advantage of the new transducer is the ability to display the two shear displacements (from either side of the specimen) individually, which permits study of aberrations in the sliding process (*e.g.*, rotations). Figure 8 illustrates the axial load vs. individual shear displacements for several representative triaxial shear tests. A, B and C are representative of most of the data collected in this program, while D is an example of some of the worst disagreement between the two individual shear displacements. Only about a half-dozen of the experiments for which data was reported were similar to example D — some half-dozen were worse, and were not reported for that reason. Aside from indicating the absence of rotation during loading, A, B and C also illustrate another interesting common feature — rotation commences, somewhat reproducibly, after sliding begins, so the two curves which are initially almost identical begin to separate. The amount of separation is roughly proportional to the distance slid, and the rotation is "permanent", in the sense that it is not recovered upon unloading. It is also interesting to note that, despite the rotation

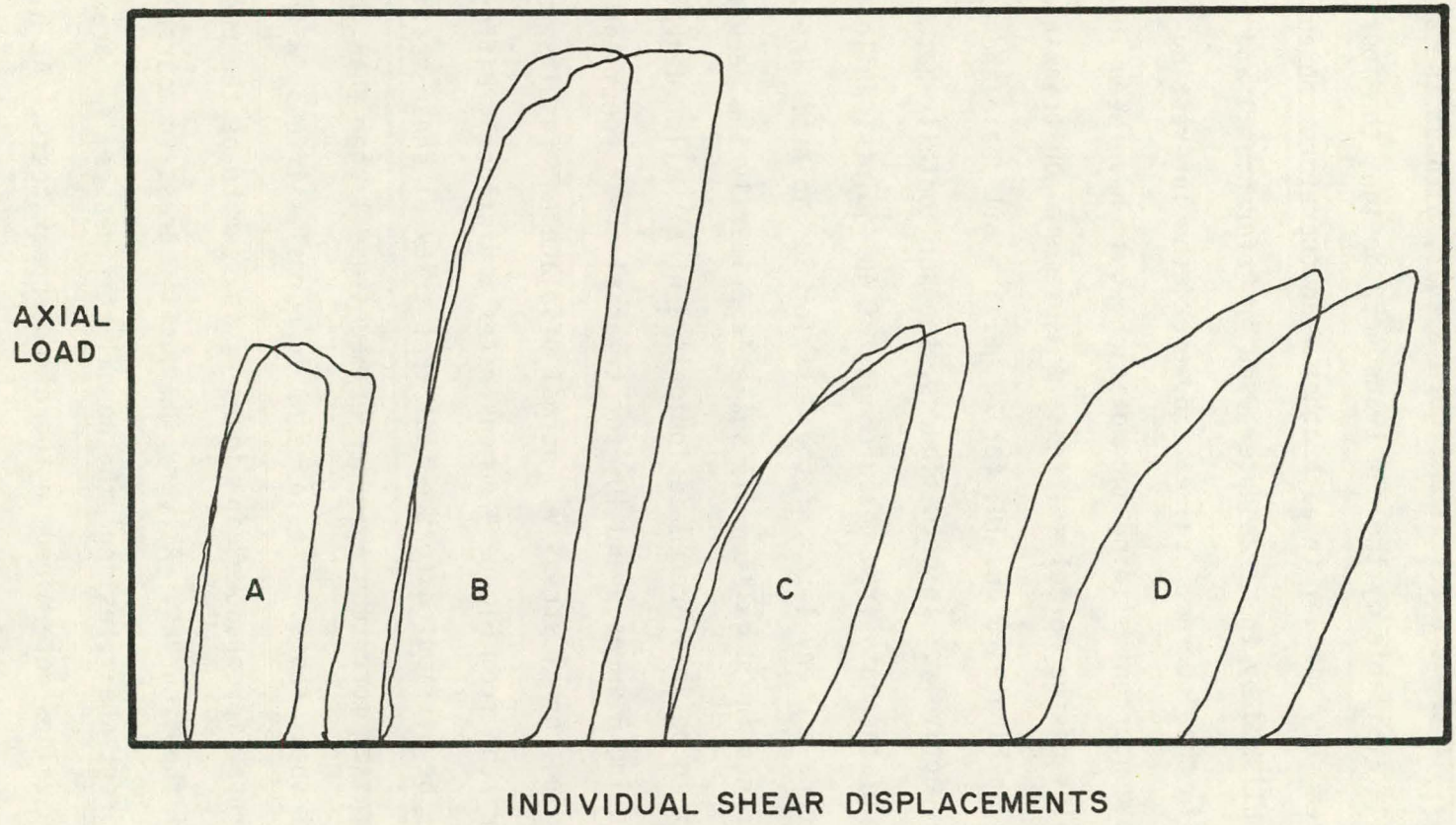

Figure 8. Representative raw data illustrating the axial load vs. shear displacement results. The two curves are those obtained from opposite sides of the specimen. A, B and C are typical of most of the results, while D is an example of some of the worst disagreement between the two individual shears.

during sliding, the unloading stiffness is virtually idential to the loading stiffness. It seems clear from Figure 8 that, without the additional information made available by the new transducer design, the four examples would have looked very similar to each other, and therefore the automatic averaging accomplished by the transducer used in References 1 and 2 would have resulted in the "correct" values. However, the interesting information about the concurrent sliding and rotation would have been lost.

Results of the normal stiffness measurements on triaxial shear specimens are shown in Figures 9 and 10, for 20 gal/ton oil shale and 40 gal/ton oil shale, respectively. In both figures, the horizontally-hatched bands are envelopes of the data from measurements of 45° joints, while the vertically-hatched bands are envelopes of the data for 30° joints. The narrower band for 30° joints in 20 gal/ton oil shale is primarily the result of fewer tests, and is not to be interpreted as indicative of a smaller degree of scatter.

Comparing Figures 9 and 10, for triaxial shear specimens, with the corresponding normal stress vs. normal displacement results for the direct shear specimens from Figure 4 demonstrates a distinctly different behavior which must be attributed to the fact that triaxial shear testing involved normal stresses more than an order of magnitude larger than those used in the direct shear tests. The increase in normal stiffness with increasing normal stress, foreshadowed in Figure 4, is seen to be the predominant feature of these curves. At very low normal stress (comparable to those used in direct shear testing) the normal stiffnesses, K_n, are comparable with those values determined in the direct shear tests. At higher stresses, however, the stiffnesses increase remarkably for both materials — to about

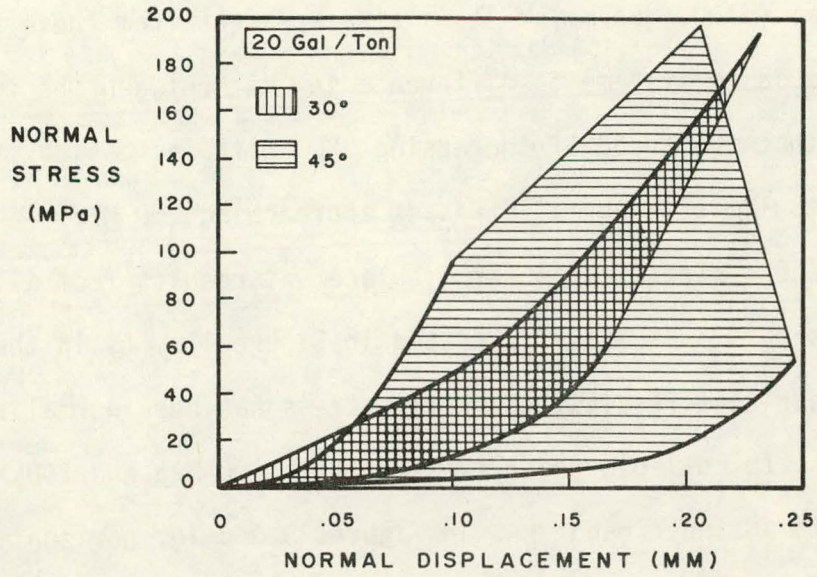

Figure 9. Normal stiffness results for 20 gal/ton oil shale triaxial shear specimens. The wider scatter band for 45° joints is simply a consequence of a larger number of tests than for the 30° joints.

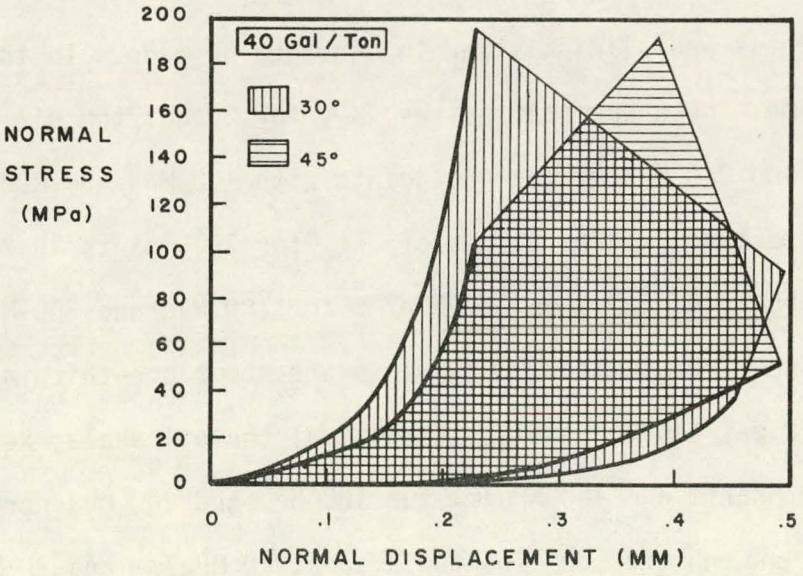

Figure 10. Normal stiffness results for 40 gal/ton oil shale triaxial shear specimens. Note that the scale is different from Figure 9.

1500 MPa/mm (±1000 MPa/mm). It is also apparent from these two figures that there is no systematic difference in K_n between the two oil shales, and also that the trend of increasing K_n with increasing stress has not reached its limit at normal stresses approaching 200 MPa.

The shear stress vs. shear displacement results from all the successful triaxial shear tests are illustrated in Figure 11. As in the case of the direct shear test results, the shear stress has been normalized by the normal stress, to collapse the curves for both 100 MPa and 200 MPa normal stress levels into a single band. As in Figures 9 and 10, horizontal hatching is used for 45° joints and vertical hatching for 30° results. The utility of the nondimensionalization is more readily seen in this figure. Again the curves are very much nonlinear, making the use of linear-elastic parameters highly approximate. However, the scatter band from several tests can be confidently approximated as linear, if desired, and useful estimates of the shear stiffness and sliding strength can then be made. In this high normal stress regime, the shear stiffnesses, K_s, for 20 gal/ton oil shale are about 120 MPa/mm and 240 MPa/mm for 45° joints with 100 MPa and 200 MPa normal stress, respectively. The values of K_s for 30° joints in 20 gal/ton oil shale are about 40 MPa/mm and 80 MPa/mm for 100 MPa and 200 MPa normal stress, respectively. Thus, 30° joints are about one-third as stiff as 45° joints in 20 gal/ton oil shale. For 40 gal/ton oil shale, K_s for 45° joints is about 80 MPa/mm and 160 MPa/mm for 100 MPa and 200 MPa normal stress, respectively, and K_s for 30° joints is about 10 MPa/mm and 20 MPa/mm for 100 MPa and 200 MPa normal stress, respectively. Therefore, 30° joints in 40 gal/ton oil shale are about one-eight as stiff as 45° joints.

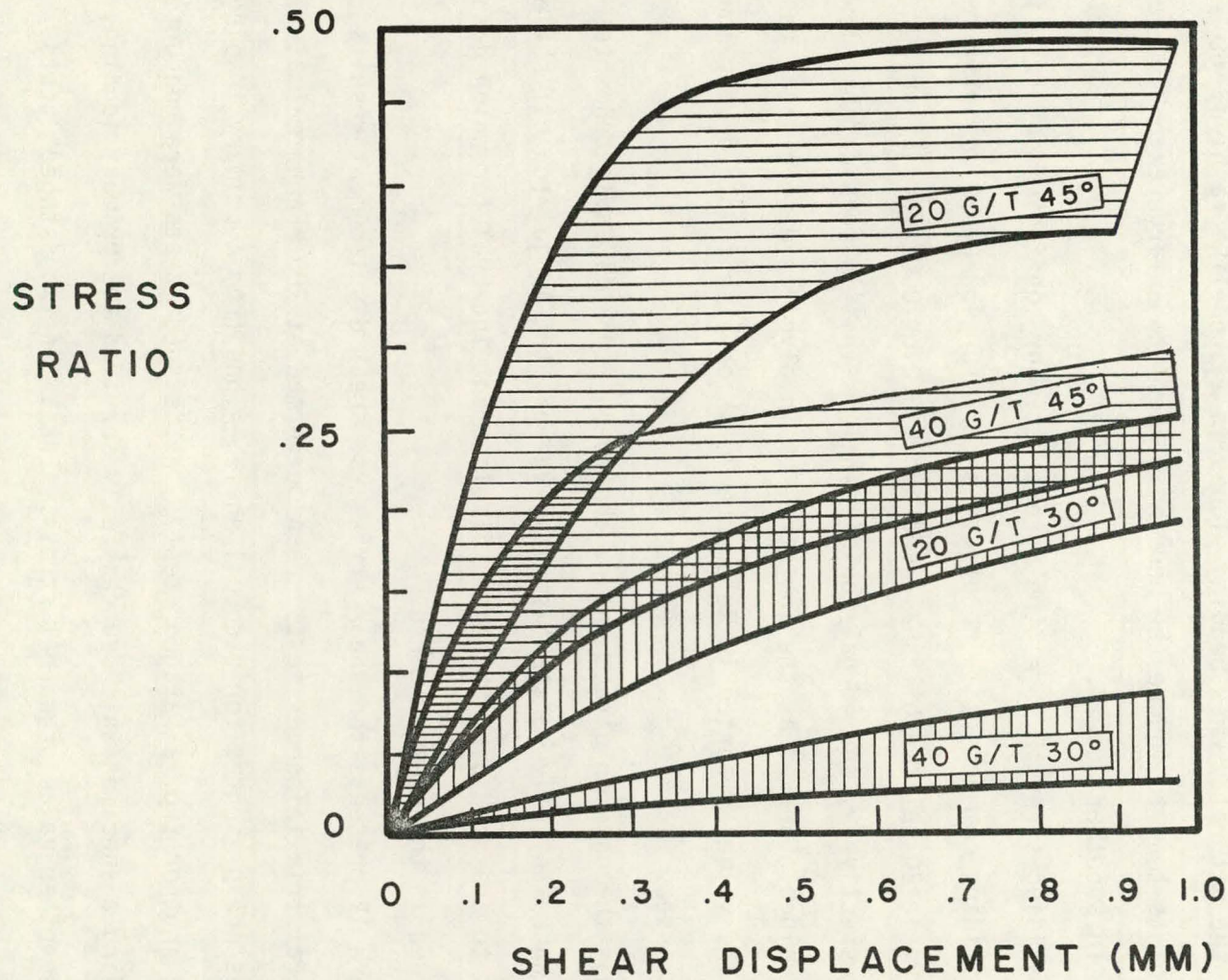

Figure 11. Shear stress/normal stress ratio vs. shear displacement results for all triaxial shear tests. 30° joints are less stiff and weaker than 45° joints in the same grade of oil shale, and 40 gal/ton oil shale is considerably weaker and more compliant than 20 gal/ton oil shale, in this high normal stress regime.

The pronounced shear stiffness difference between 30° and 45° joints observed here may be due to the tendency for the 45° joints to form by following the naturally weak bedding planes in a step-like fashion, while the 30° joints tend to ignore the bedding planes (to a large extent), resulting in smoother joints.

The sliding strength (*i.e.*, the stress ratio or coefficient of friction at which sliding commences) is about 0.4 or 0.2 for 45° or 30° joints, respectively, in 20 gal/ton oil shale and about 0.2 or 0.02 for 45° or 30° joints, respectively, for 40 gal/ton oil shale. This is considerably lower than the values observed at the low stresses involved in direct shear testing, and the values reported in Reference 2, which also involved very low normal stresses.

As was the case in direct shear, the 20 gal/ton oil shale tends to slide at an essentially constant stress, whereas the 40 gal/ton oil shale continues to "harden" over the shear displacement interval for which data was recorded in these experiments.

Figure 12 presents the shear stress vs. shear displacement results from several triaxial shear tests, each performed at 200 MPa normal stress. Two curves are presented for each oil shale — one from a primary loading test, and another from a "staged" test. The "staged" tests were conducted by reloading a specimen which successfully survived the primary loading, but at the other value of normal stress. Thus, the two "staged" tests shown here were previously sheared at 100 MPa normal stress. The loading-unloading-reloading cycles performed on these specimens show that the unloading and reloading stiffness values are not materially changed by

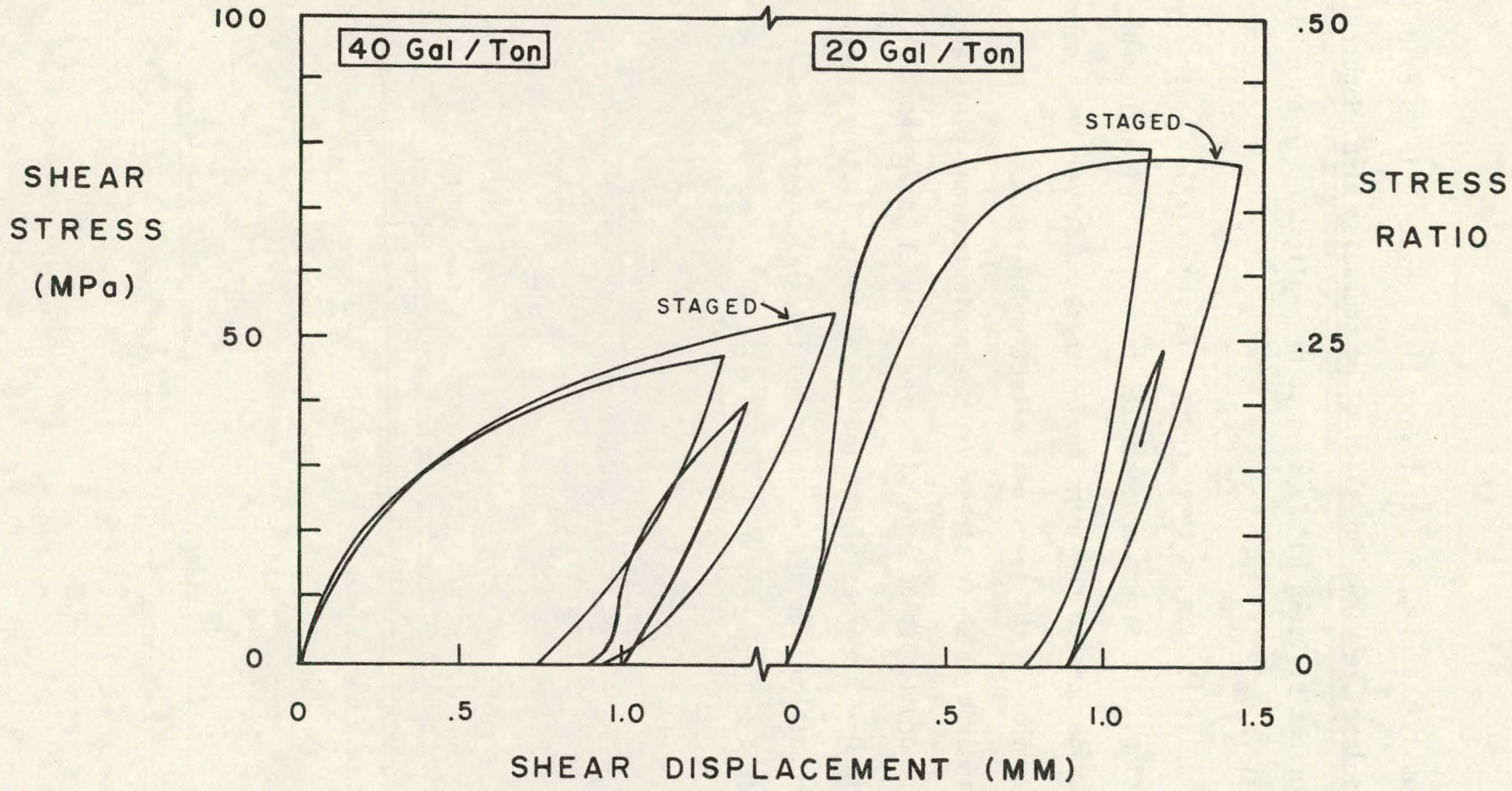

Figure 12. Shear stress vs. shear displacement curves for four 45° joints at 200 MPa normal stress, illustrating the difference in stiffness and strength between 20 gal/ton and 40 gal/ton oil shale and the negligible effect of staging on the joint properties. Note that unloading and reloading below the sliding strength shows relatively little nonlinearity and hysteresis.

the previously shearing, and that very little hysteresis is evident (below the stress level required for sliding, of course). Also, Figure 12 shows that the effect of "staging" is seen to be negligible, in both 20 and 40 gal/ton oil shale.

Figure 13 illustrates three representative triaxial shear specimens, after testing. The figure demonstrates that there is considerably more surface damage done to the joint during these relatively high normal stress experiments than in the low stress direct shear tests.

The individual shear stress vs. shear displacement plots and normal stress vs. normal displacement plots for triaxial shear tests are contained in Appendix D. Summaries of the individual tests, listing specimen numbers and test conditions for direct shear and triaxial shear tests are contained in Appendix A and Appendix B, respectively.

Figure 13. Representative joint surfaces after triaxial shear testing. Comparison with Figure 5 illustrates the greater degree of surface asperity crushing which occurs at the higher stress levels used in the triaxial shear tests.

CONCLUSIONS

The main conclusions from the experimental work are as follows:

1. In direct shear, K_n is fairly constant — ∿50 MPa/mm for 20 gal/ton oil shale and ∿10 MPa/mm for 40 gal/ton oil shale, with some evidence of stiffening with increasing stress in the rich shale.

2. In the low normal stress regime (*i.e.*, direct shear), K_s is initially ∿125 MPa/mm and ∿70 MPa/mm for 20 gal/ton and 40 gal/ton oil shale, respectively, although the shear stress vs. shear displacement relationship is considerably nonlinear, even at low shear stresses. In triaxial shear, K_n is initially very low — comparable with the values obtained in direct shear — but then K_n increases dramatically to ∿1500 MPa/mm (±1000 MPa/mm) with increasing normal stress. The difference in K_n for the two kerogen contents is within the range of scatter in K_n for either of the shales.

3. In the low normal stress regime, sliding commences at a stress ratio of about unity for both kerogen contents, although the richer shale has a higher coefficient of friction and continues to "harden" during sliding, while the 20 gal/ton shale slides at a constant coefficient of friction. In the high normal stress regime, sliding commences at a stress ratio of about 0.4 or 0.2 for 45° and 30° joints, respectively, in 20 gal/ton oil shale and at about 0.2 or 0.02 for 45° and 30° joints, respectively, in 40 gal/ton oil shale.

4. 40 gal/ton oil shale exhibits more nonlinearity and more scatter and continues to "harden" more during sliding than 20 gal/ton oil shale.

5. Unloading-reloading cycles, below the stress required for sliding, indicate only a small amount of hysteresis and very little stiffness decay.

6. "Staging", in triaxial shear, has no measurable effect upon K_n, K_s or sliding strength.

7. Direct shear and triaxial shear tests were performed at normal stresses below 10 MPa and over 100 MPa respectively. Whereas comparable K_n and K_s were obtained at similar normal stresses, distinctly different behavior was observed at higher normal stresses; K_n is increased between one and two orders of magnitude and the coefficient of friction is very much reduced.

REFERENCES

1. Rosso, R. S., "A Comparison of Joint Stiffness Measurements in Direct Shear, Triaxial Compression, and *In Situ*", *Int. J. Rock Mech. Min. Sci. & Geomech. Abstr., Vol. 13,* pp. 167-172, Pergamon Press 1976.

2. Rosso, R. S., Simonson, E. R., Wawersik, W. R., and Jones, A. H., "Determination of the Properties of a Jointed Oil Shale", Terra Tek, Inc., Report TR 74-60 (December 1974).

APPENDIX A

JOINTED OIL SHALE DIRECT SHEAR TEST SUMMARY

Sequence No.	Test ID	Normal Stress (MPa)	Strain Rate*	Comments
9	120A	2.2	S	Shear stiffness, 1st loading
10	220A	8.8	S	Shear stiffness, 1st loading
11	240A	2.2	S	Shear stiffness, 1st loading
12	420A	2.2	S	Shear stiffness, 1st loading
13	420BF	8.8	F	Shear stiffness, 2nd loading
14	320A	6.6	S	Shear stiffness, 1st loading
15	340AN	-	-	Normal stiffness, 1st loading
16	340A	8.8	S	Shear stiffness, 1st loading
17	340BN	-	-	Normal stiffness, 2nd loading
18	340CN	-	-	Normal stiffness, 3rd loading
19	340CF	8.8	F	Shear stiffness, 3rd loading
20	520AN	-	-	Normal stiffness, 1st loading
21	520A	4.4	S	Shear stiffness, 1st loading
22	440AN	-	-	Normal stiffness, 1st loading
23	440A	4.4	S	Shear stiffness, 1st loading
24	620AN	-	-	Normal stiffness, 1st loading
25	620AF	4.4	F	Shear stiffness, 1st loading
26	540AN	-	-	Normal stiffness, 1st loading
29	540A	6.6	S	Shear stiffness, 1st loading
30	640AN	-	-	Normal stiffness, 1st loading
31	640AF	8.8	F	Shear stiffness, 1st loading
32	720AN	-	-	Normal stiffness, 1st loading
33	720A	8.8	S	Shear stiffness, 1st loading
34	740A	8.8	S	Shear and normal stiffness, 1st loading
35	840A	4.4	S	Shear and normal stiffness, 1st loading

*Slow or Fast

THIS PAGE

WAS INTENTIONALLY

LEFT BLANK

APPENDIX B

JOINTED OIL SHALE TRIAXIAL SHEAR TEST SUMMARY

Shear Stiffness - 20 Gal/Ton

Specimen	Test ID	Normal Stress (MPa)	Joint Angle	Comments
1	14520D	100	45°	Some initial rotation; good
2	14520E	100	45°	Good
2	24520ES	200	45°	Good - Staged test
4	14520A	100	45°	Leaked
7	24520A	200	45°	Yielded before sliding
8	14520B	100	45°	Some initial rotation; good
10	14520C	100	45°	Good
13	14520F	100	45°	Good; loaded twice with good agreement
14	14520G	100	45°	Good
15	24520B	200	45°	Leaked
16	14520H	100	45°	Leaked
17	13020A	100	30°	Good
17	23020AS	200	30°	Some initial rotation; good - staged test
18	13020C	100	30°	Good rotation; no good
19	13020B	100	30°	Good
20	23020B	200	30°	Good
20	13020AS	100	30°	Good - staged test
21	23020B	200	30°	Some initial rotation; good
22	24520C	200	45°	Good; unloading
22	14520AS	100	45°	Good; unloading - staged test
23	14520I	100	45°	Good; unloading
23	24520BS	200	45°	Good; unloading - staged test

APPENDIX B - Continued

Shear Stiffness Tests - 40 Gal/Ton

Specimen	Test ID	Normal Stress (MPa)	Joint Angle	Comments
50	13040A	100	30°	Leaked
51	13040B	100	30°	Good
52	13040C	100	30°	Good
52	23040AS	200	30°	Good - staged test
53	23040A	200	30°	Good
53	13040AS	100	30°	Gross rotation; no good - staged test
54	23040B	200	30°	Good
55	13040D	100	30°	Good
56	24540A	200	45°	Good, unloading
57	14540B	100	45°	Good; unloading
57	24540BS	200	45°	Some rotation; good; unloading - staged test
58	24540B	200	45°	Leaked
59	14540A	100	45°	Good
59	24540AS	200	45°	Leaked - staged test

Normal Stiffness Tests - 20 Gal/Ton

Specimen	Test ID	Joint Angle	Comments
16	14520HN	45°	First loading - leaked
17	13020AN	30°	First loading
17	23020ASN	30°	Second loading
18	13020CN	30°	First loading
19	13020BN	30°	First loading
20	23020AN	30°	First loading
20	13020ASN	30°	Second loading
21	23020BN	30°	First loading
22	24520CN	45°	First loading
22	14520ASN	45°	Second loading
23	14520IN	45°	First loading
23	24520BSN	45°	Second loading

Normal Stiffness Tests - 40 Gal/Ton

Specimen	Test ID	Joint Angle	Comments
50	13040AN	30°	First loading - leaked
51	13040BN	30°	First loading
52	13040CN	30°	First loading
52	23040ASN	30°	Second loading
53	23040AN	30°	First loading
53	13040ASN	30°	Second loading
54	23040BN	30°	First loading
55	13040DN	30°	First loading
56	24540AN	45°	First loading
57	14540BN	45°	First loading
57	24540BSN	45°	Second loading
58	24540BN	45°	First loading - leaked
59	14540AN	45°	First loading
59	24540ASN	45°	Second loading - leaked

THIS PAGE

WAS INTENTIONALLY

LEFT BLANK

APPENDIX C

DIRECT SHEAR RESULTS

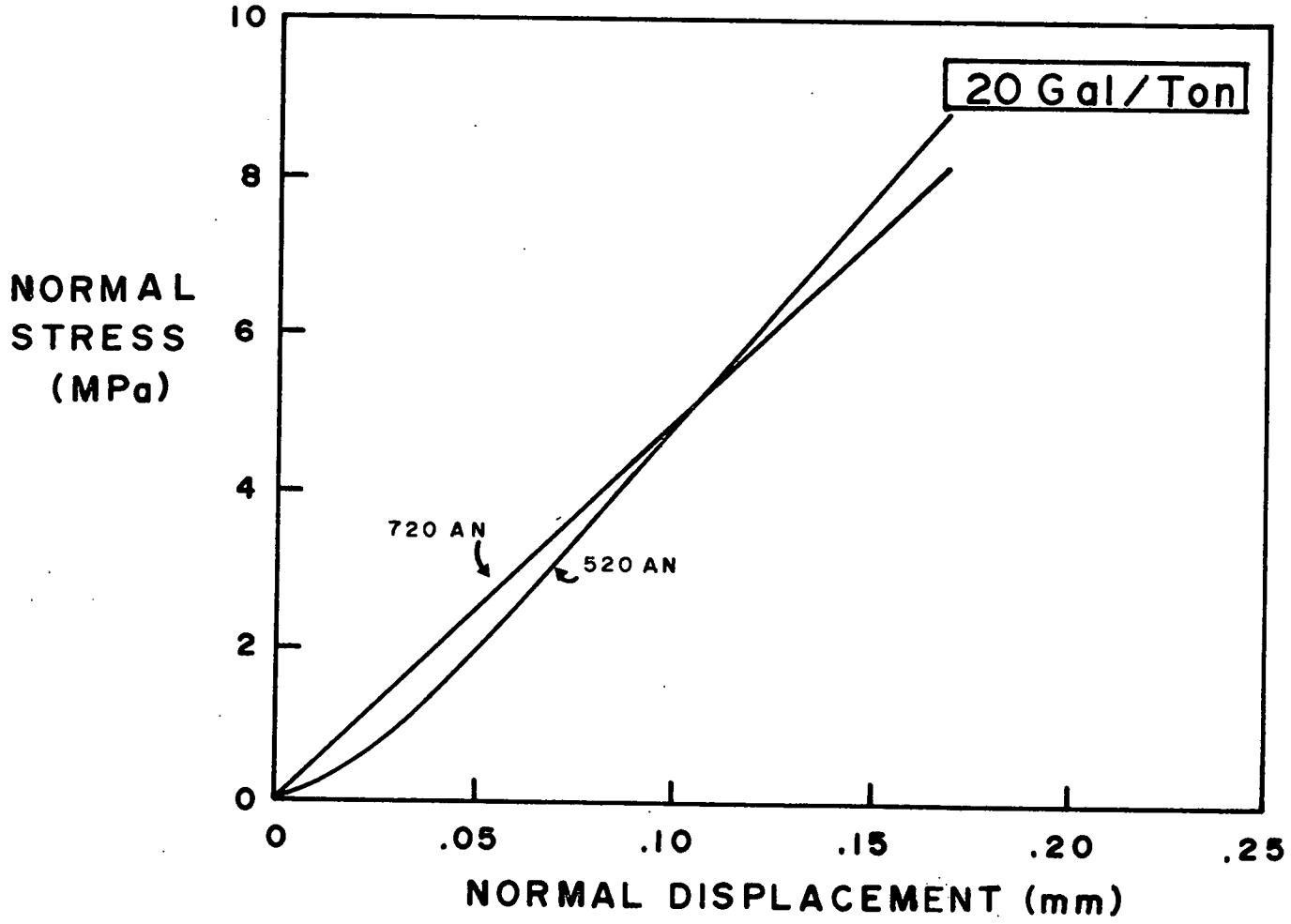

Figure C-1. Normal stiffness results for 20 gal/ton oil shale direct shear specimens.

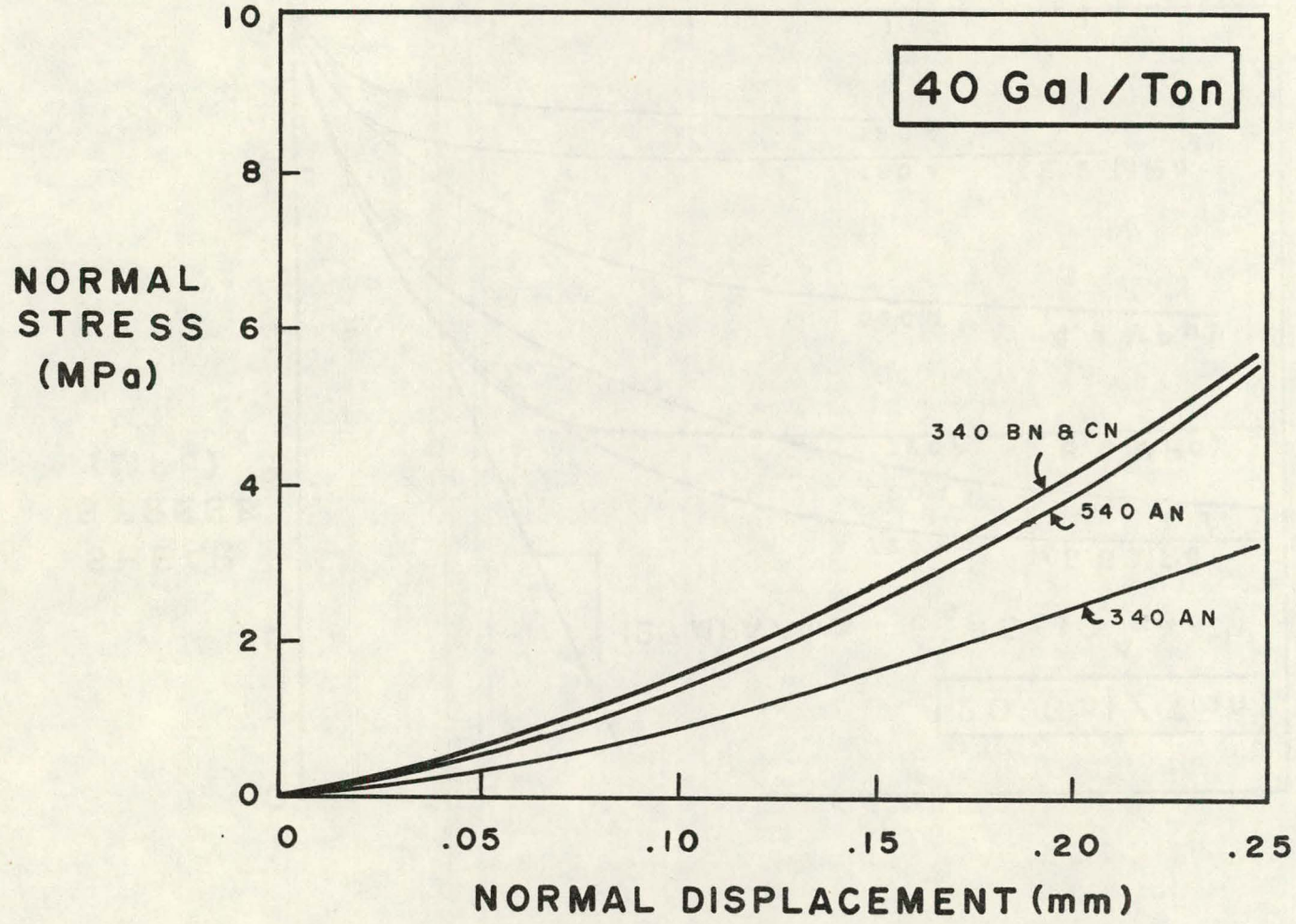

Figure C-2. Normal stiffness results for 40 gal/ton oil shale direct shear specimens.

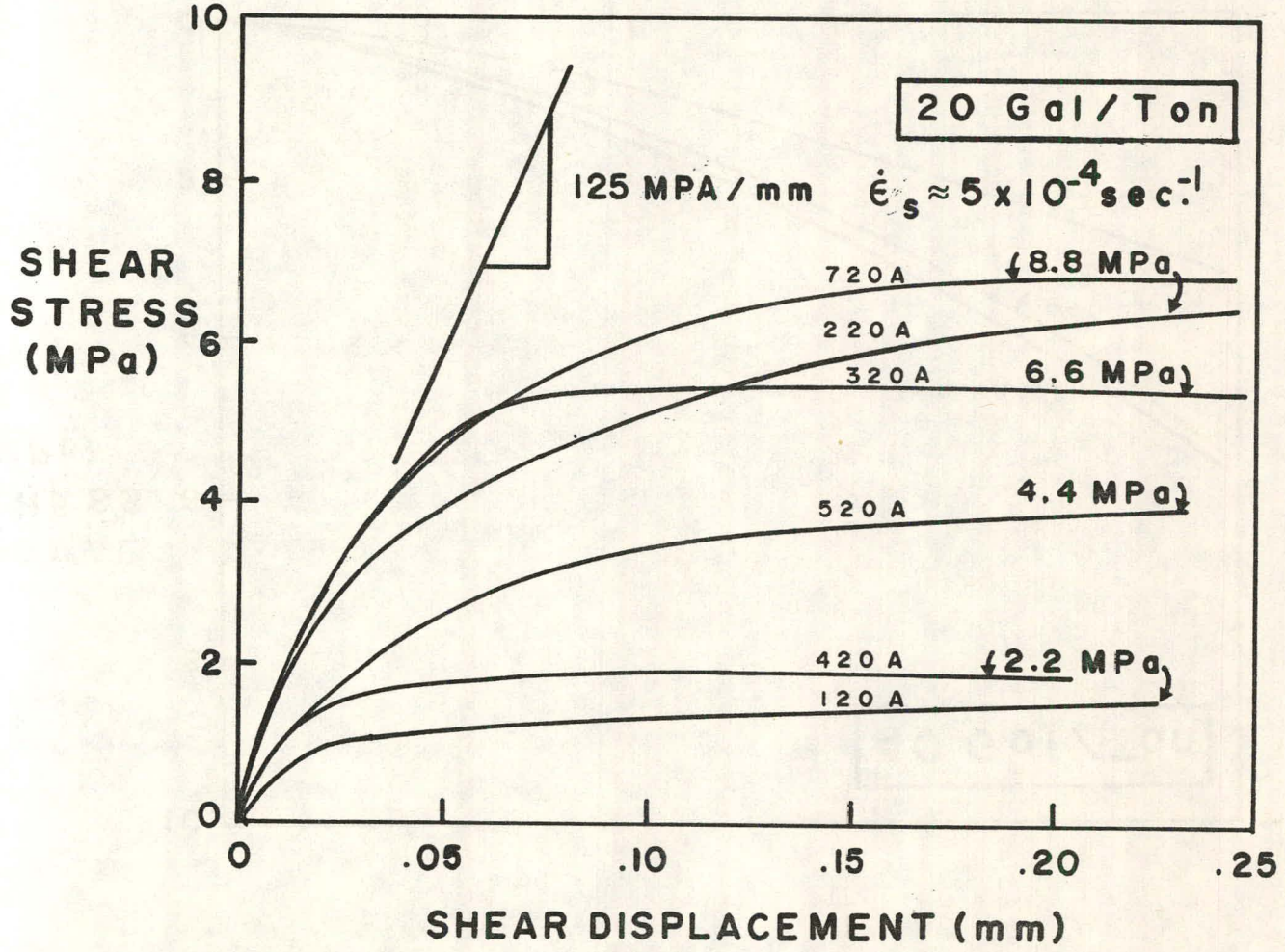

Figure C-3. Shear stress vs. shear displacement results for 20 gal/ton oil shale direct shear tests at an average strain rate of 5×10^{-4} sec^{-1}.

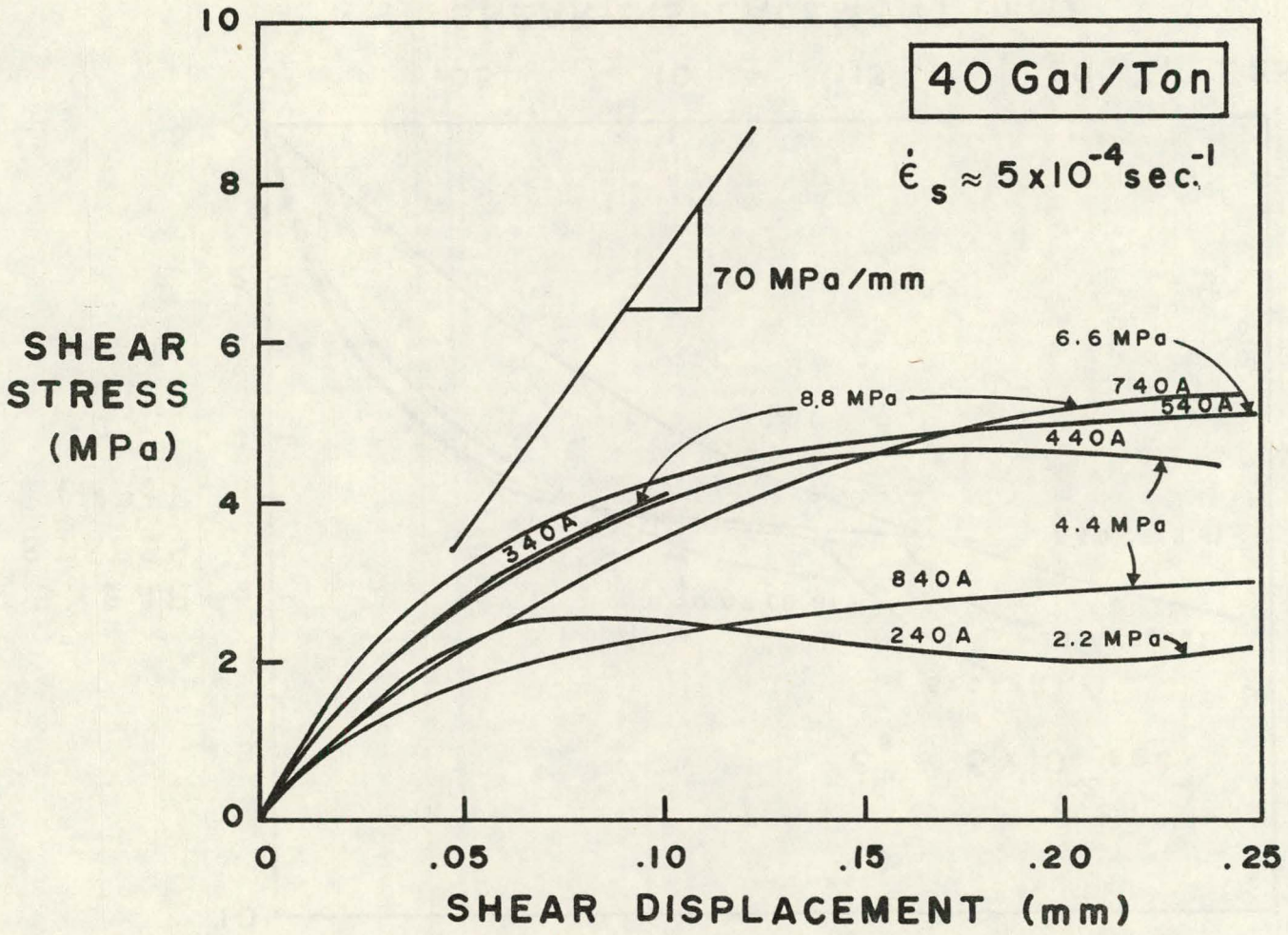

Figure C-4. Shear stress vs. shear displacement results for 40 gal/ton oil shale direct shear tests at an average strain rate of 5 x 10^{-4} sec^{-1}.

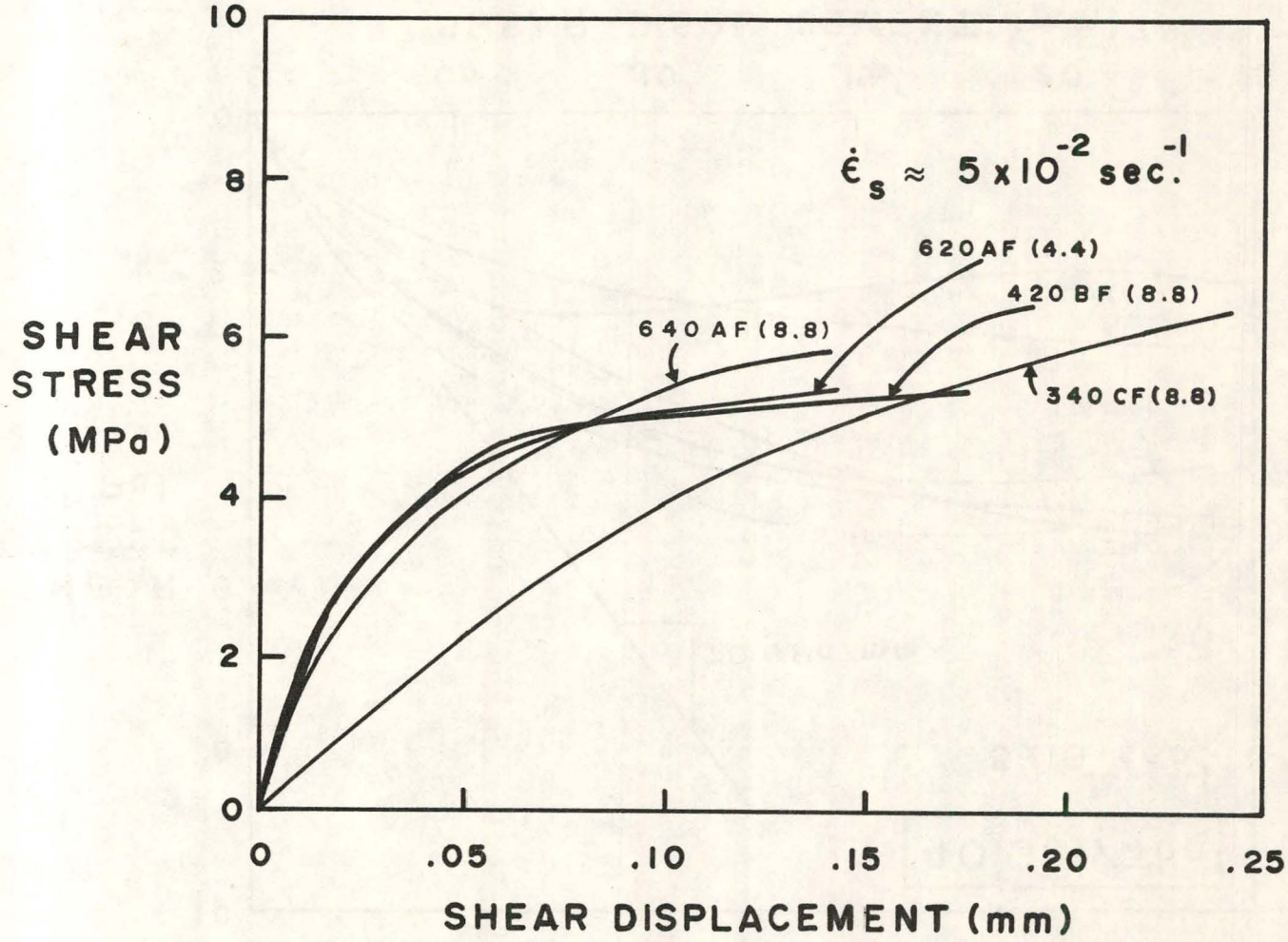

Figure C-5. Shear stress vs. shear displacement results for 20 and 40 gal/ton oil shale direct shear tests at an average strain rate of 5×10^{-2} sec^{-1}.

APPENDIX D

TRIAXIAL SHEAR RESULTS

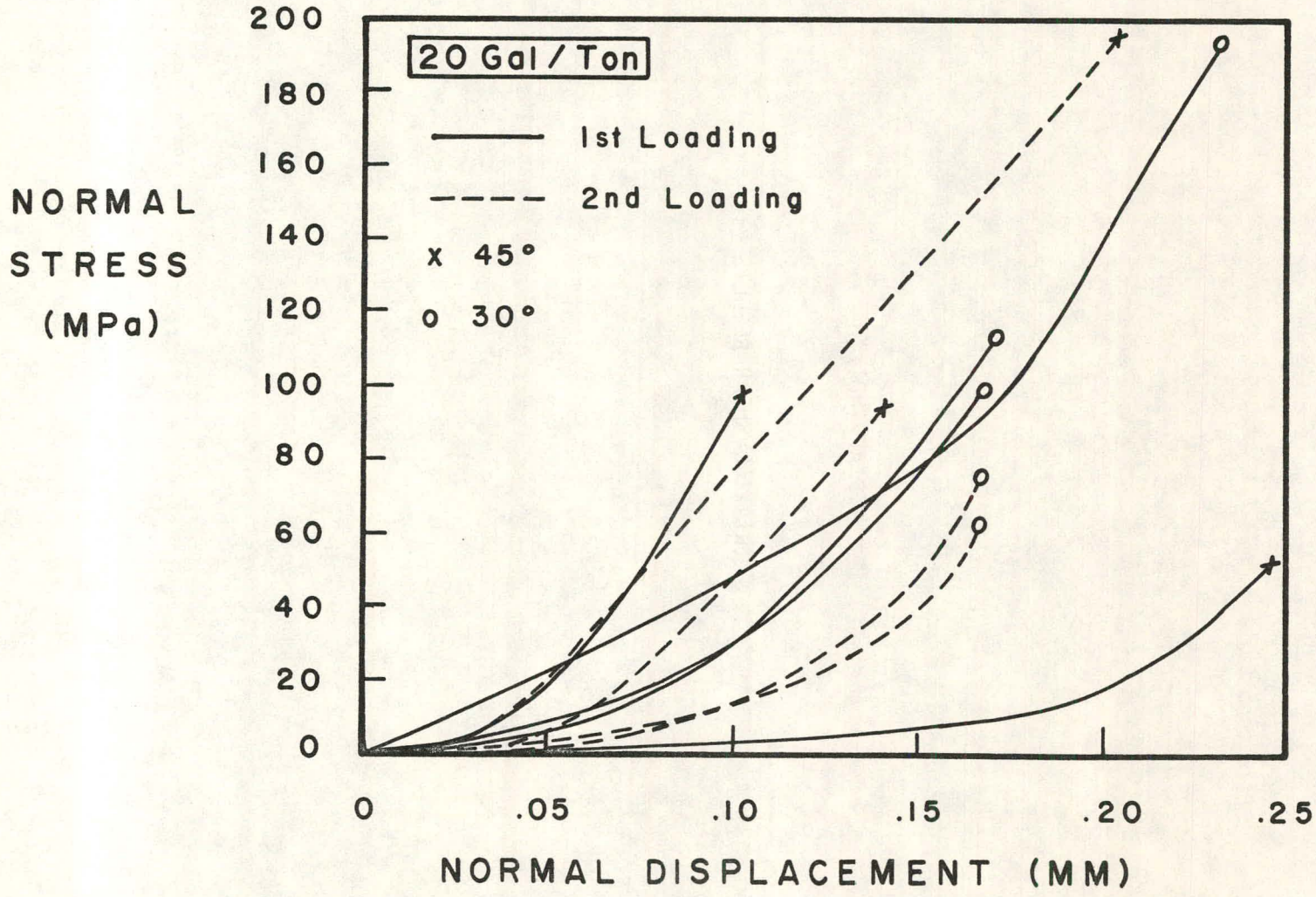

Figure D-1. Normal stiffness results for 20 gal/ton oil shale triaxial shear specimens.

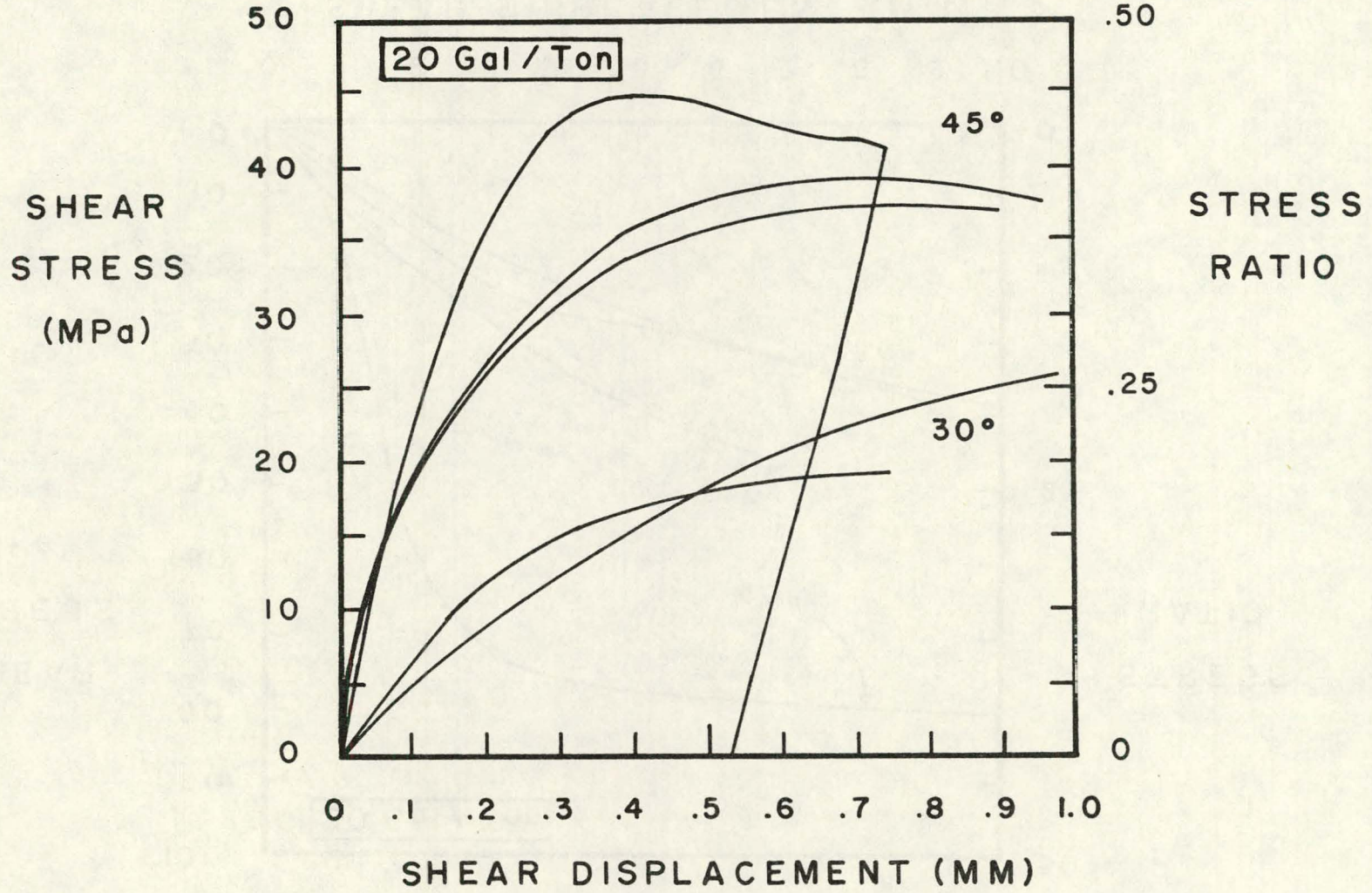

Figure D-2. Shear stress vs. shear displacement results for 20 gal/ton oil shale triaxial shear tests, with 100 MPa normal stress.

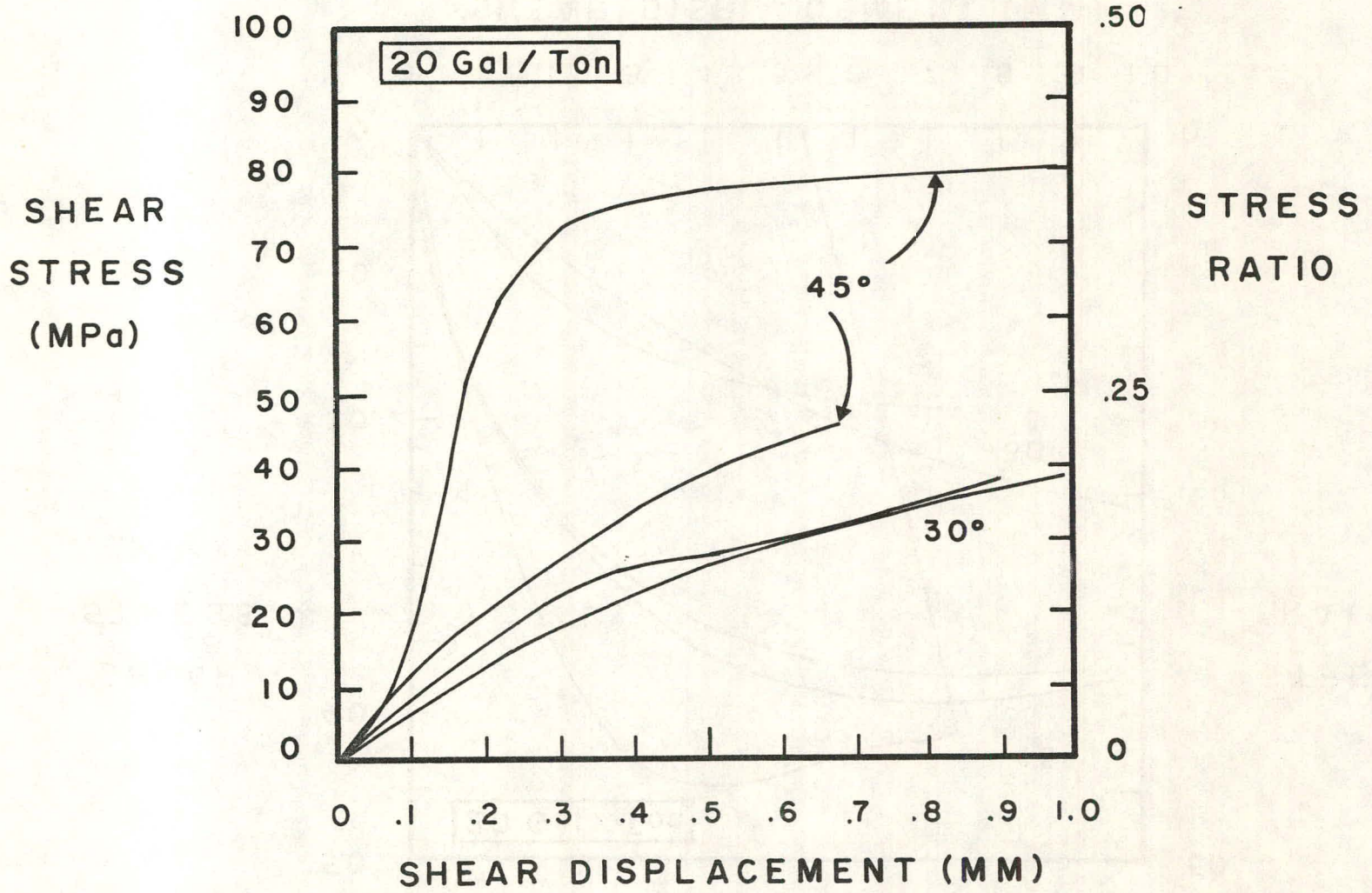

Figure D-3. Shear stress vs. shear displacement results for 20 gal/ton oil shale triaxial shear tests, with 200 MPa normal stress.

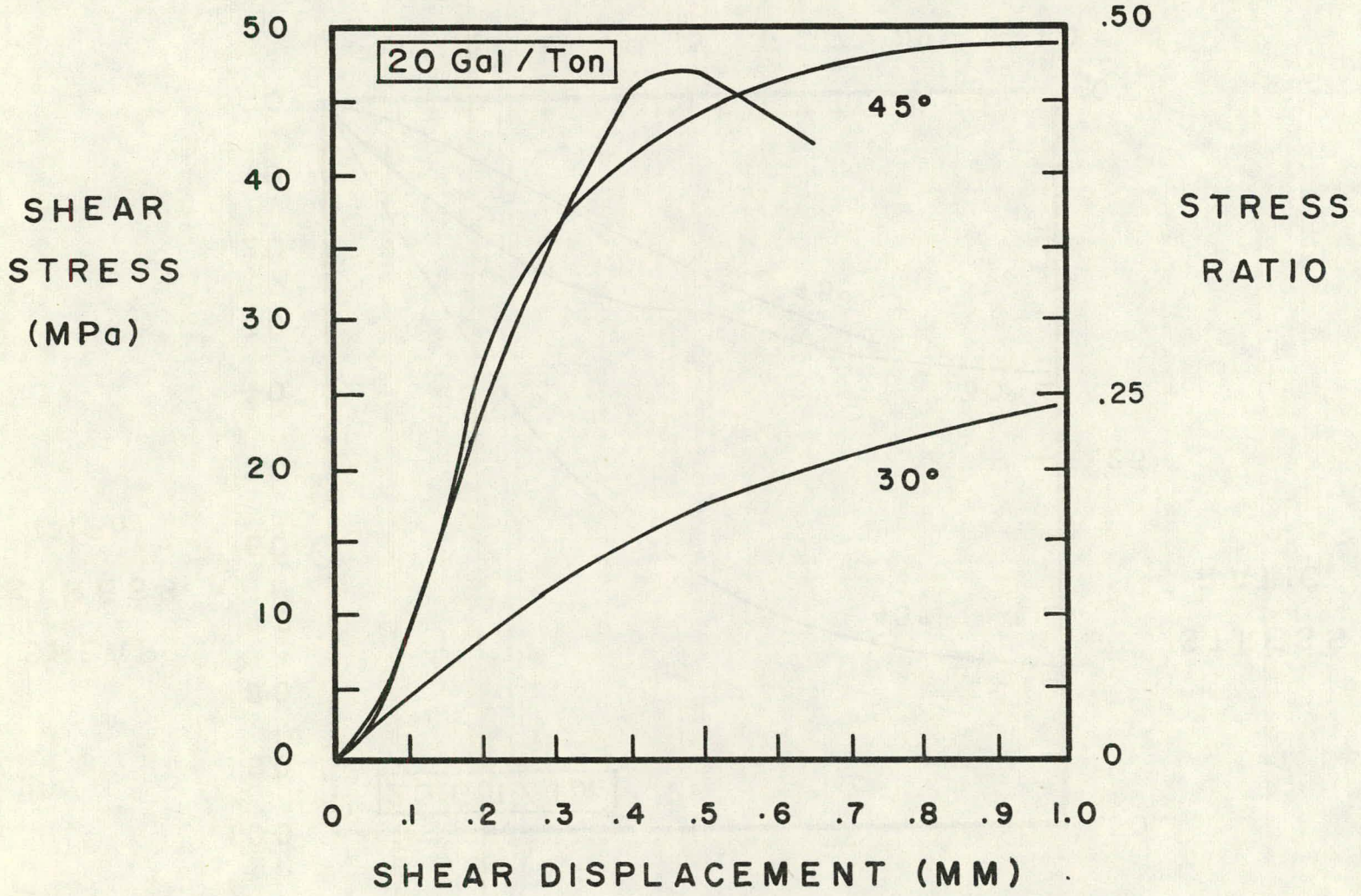

Figure D-4. Shear stress vs. shear displacement results for 20 gal/ton oil shale triaxial shear tests, with 100 MPa normal stress. These are "staged" tests, on specimens previously tested at 200 MPa normal stress.

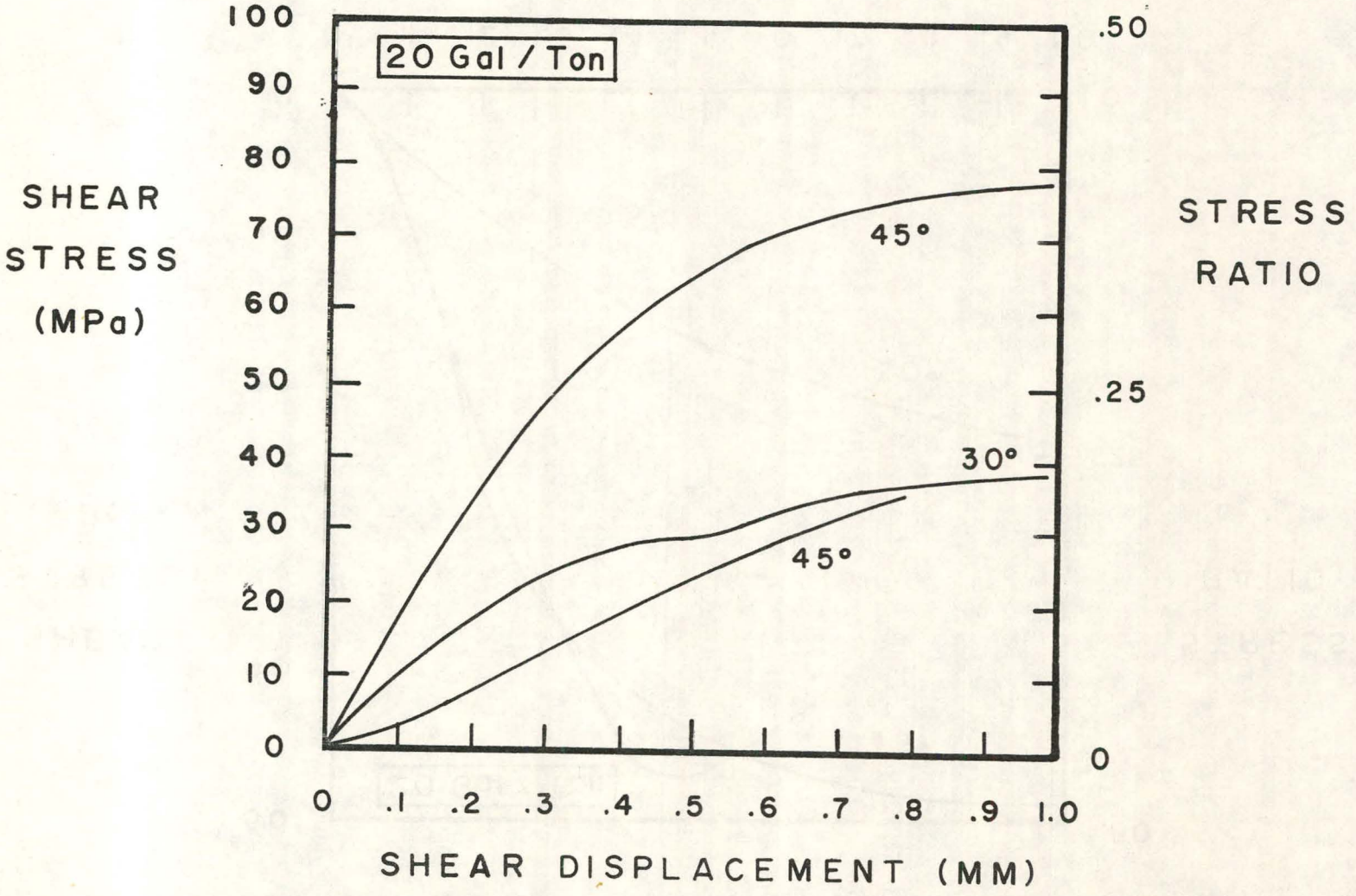

Figure D-5. Shear stress vs. shear displacement results for 20 gal/ton oil shale triaxial shear tests, with 200 MPa normal stress. These are "staged" tests, on specimens previously tested at 100 MPa normal stress.

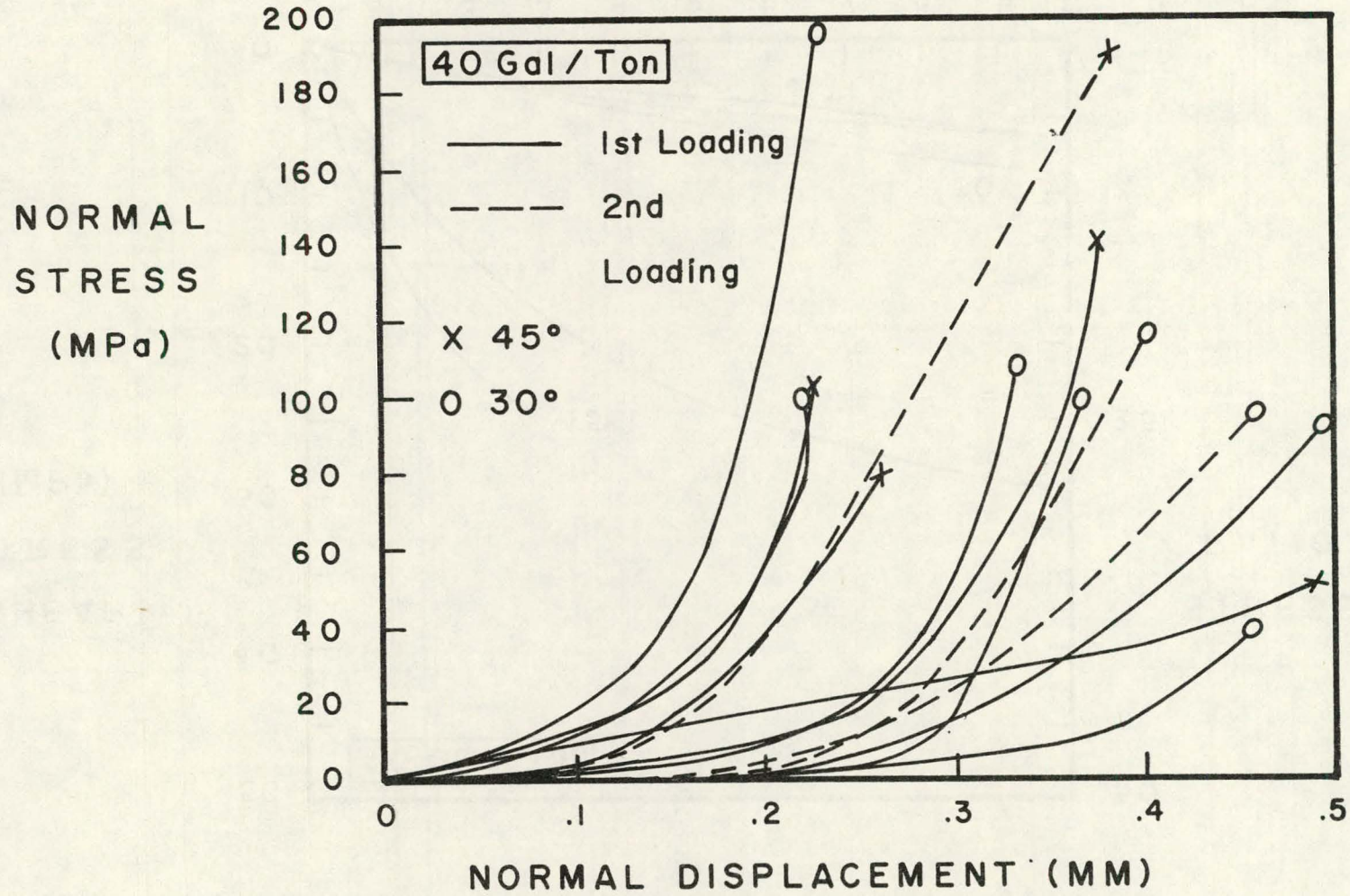

Figure D-6. Normal stiffness results for 40 gal/ton oil shale triaxial shear specimens.

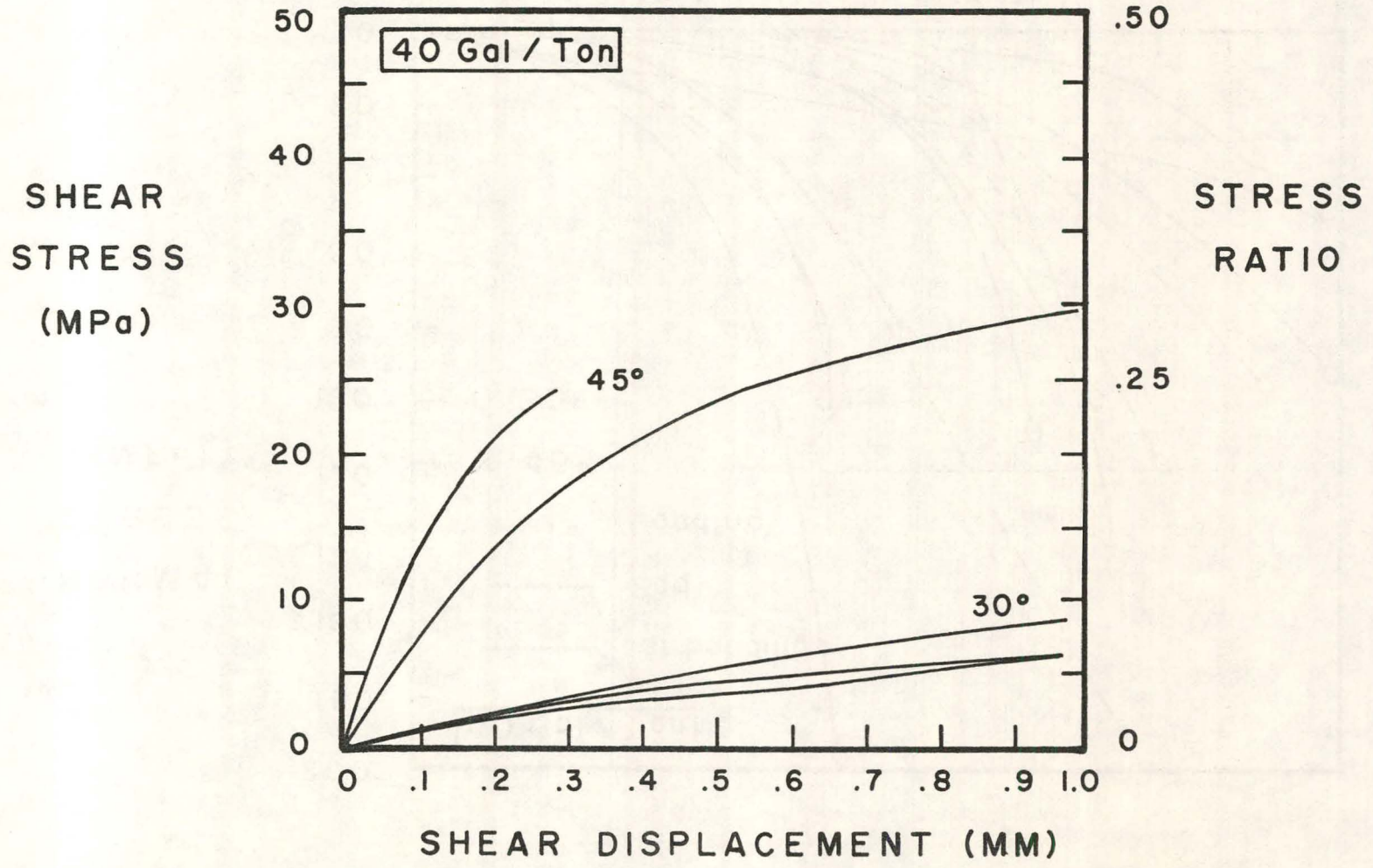

Figure D-7. Shear stress vs. shear displacement results for 40 gal/ton oil shale triaxial shear tests, with 100 MPa normal stress.

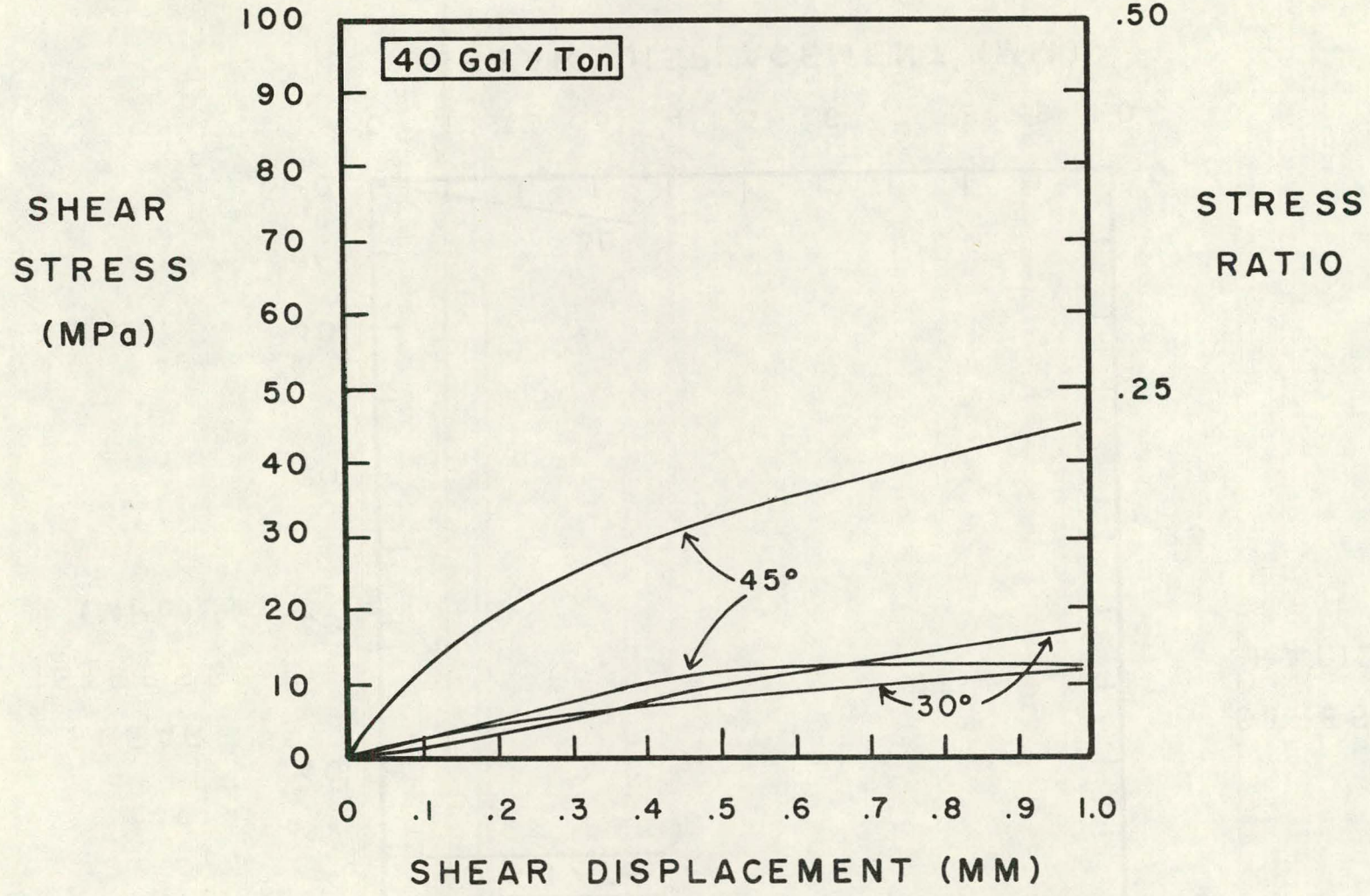

Figure D-8. Shear stress vs. shear displacement results for 40 gal/ton oil shale triaxial shear tests, with 200 MPa normal stress.

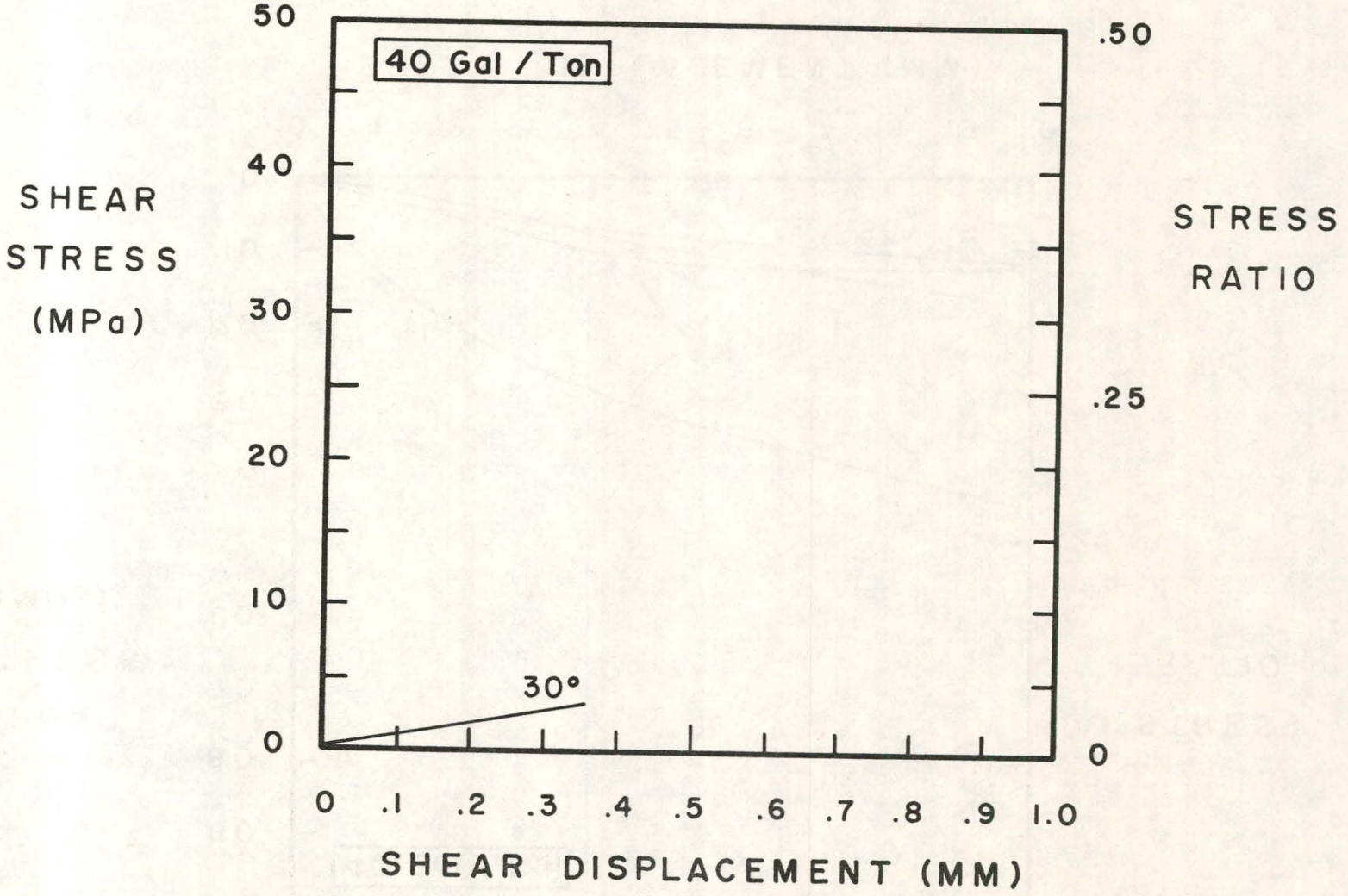

Figure D-9. Shear stress vs. shear displacement results for 40 gal/ton oil shale triaxial shear tests, with 100 MPa normal stress. These are "staged" tests, on specimens previously tested at 200 MPa normal stress.

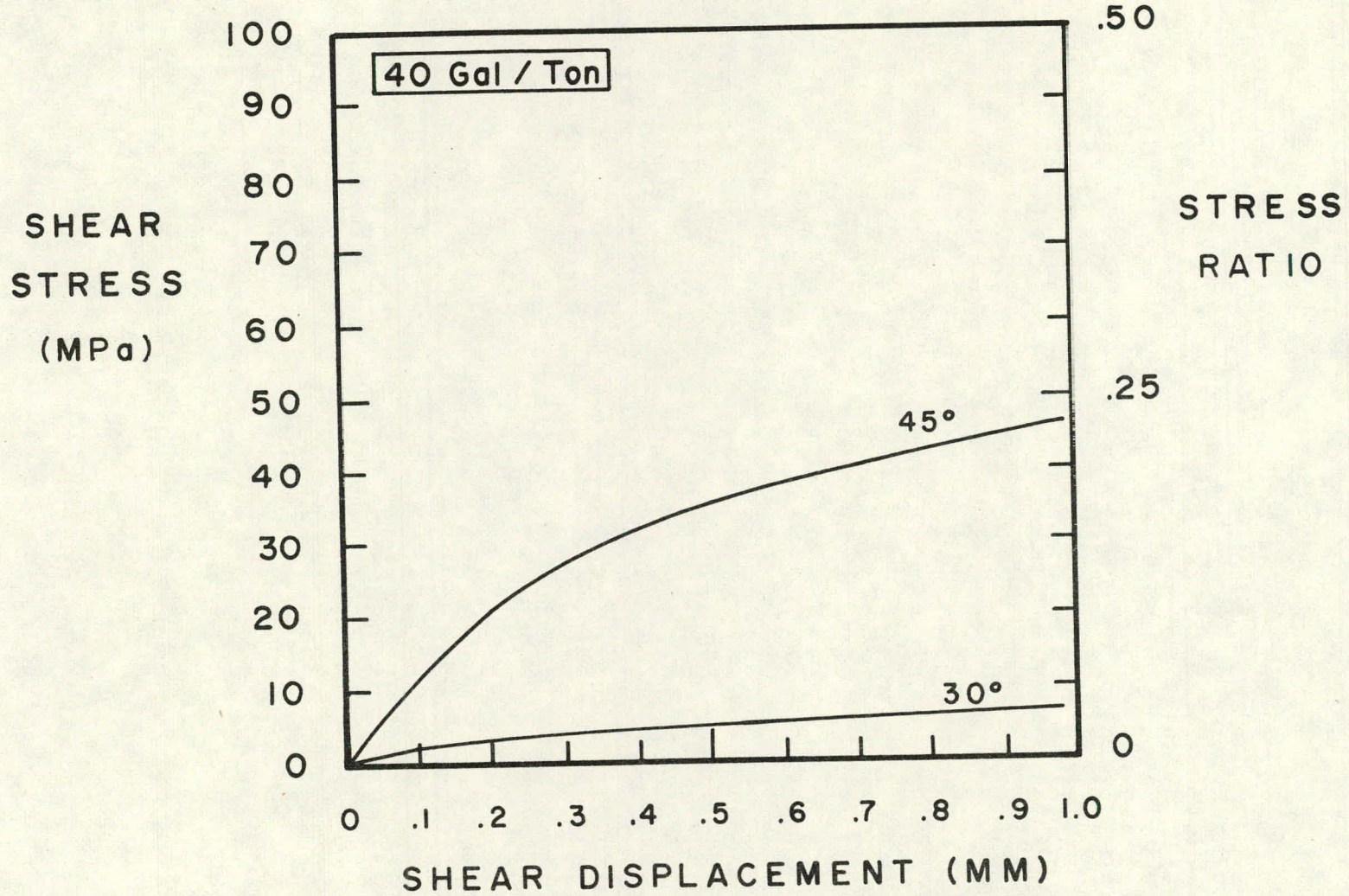

Figure D-10. Shear stress vs. shear displacement results for 40 gal/ton oil shale triaxial shear tests, with 200 MPa normal stress. These are "staged' tests, on specimens previously tested at 100 MPa normal stress.

THIS PAGE

WAS INTENTIONALLY

LEFT BLANK

DISTRIBUTION LIST

U. S. Department of Energy
Bethesda Technical Library
Washington, DC 20545

U. S. Department of Energy
DOE Library
Washington, DC 20545

U. S. Department of Energy
Albuquerque Operations Office
P. O. Box 5400
Albuquerque, NM 87115

Dr. Paul R. Wieber
Asst Director for Oil Shale
and In Situ Technology
U. S. Department of Energy
20 Massachusetts Avenue, NW
Washington, DC 20545

Mr. H. Guthrie, Director
Oil, Gas, Shale and
In Situ Technology
U. S. Department of Energy
20 Massachusetts Avenue, NW
Washington, DC 20545

Mr. Jerry Ramsey
Oil, Gas, Shale and
In Situ Technology
U. S. Department of Energy
20 Massachusetts Avenue, NW
Washington, DC 20545

Mr. L. M. Burman
Oil, Gas, Shale and
In Situ Technology
U. S. Department of Energy
20 Massachusetts Avenue, NW
Washington, DC 20545

Mr. H. E. Thomas
Oil, Gas, Shale and
In Situ Technology
U. S. Department of Energy
20 Massachusetts Avenue, NW
Washington, DC 20545

Laramie Energy Research Center (7)
U. S. Department of Energy
Laramie, WY 82070
ATTN: J. Ward Smith
H. C. Carpenter
H. B. Jensen
A. Long
R. Kerr
R. E. Paulson

Los Alamos Scientific Laboratory
Los Alamos, NM 87544
ATTN: W. J. Carter, M-6
J. Johnson, T-4

Dr A. E. Lewis
Lawrence Livermore Laboratory
University of California
P. O. Box 808
Livermore, CA 94550

Sandia Laboratories (12)
Albuquerque, NM 87115
ATTN: 5100 J. K. Galt
5160 W. Herrmann
5162 M. E. Kipp
5163 D. E. Munson
5163 K. W. Schuler
5434 R. R. Neel
5710 G. E. Brandvold
5730 H. M. Stoller
5734 A. L. Stevens
5734 R. R. Boade
5732 R. A. Schmidt

Prof. M. P. Cleary
Massachusetts Institute of Technology
Room 3-356
77 Massachusetts Avenue
Cambridge, MA 02139

Prof. A. R. Ingraffea
Civil Engineering Department
Cornell University
Ithaca, NY 14853